

RailX: A Flexible, Scalable, and Low-Cost Network Architecture for Hyper-Scale LLM Training Systems

Yinxiao Feng
Tsinghua University
fyx20@mails.tsinghua.edu.cn

Tiancheng Chen
ETH Zurich
tiancheng.chen@inf.ethz.ch

Yuchen Wei
Tsinghua University
weiy22@mails.tsinghua.edu.cn

Siyuan Shen
ETH Zurich
siyuan.shen@inf.ethz.ch

Shiju Wang
Beihang University
21373455@buaa.edu.cn

Wei Li
Tsinghua University
liw21@mails.tsinghua.edu.cn

Kaisheng Ma*
Tsinghua University
kaisheng@mail.tsinghua.edu.cn

Torsten Hoefler
ETH Zurich
torsten.hoefler@inf.ethz.ch

ABSTRACT

Increasingly large AI workloads are calling for hyper-scale infrastructure; however, traditional interconnection network architecture is neither scalable nor cost-effective enough. Tree-based topologies such as the *Rail-optimized* network are extremely expensive, while direct topologies such as *Torus* have insufficient bisection bandwidth and flexibility. In this paper, we propose *RailX*, a reconfigurable network architecture based on intra-node direct connectivity and inter-node circuit switching. Nodes and optical switches are physically 2D-organized, achieving better scalability than existing centralized circuit switching networks. We propose a novel interconnection method based on *Hamiltonian Decomposition* theory to organize separate rail-based rings into *all-to-all* topology, simultaneously optimizing ring-collective and all-to-all communication. More than 100K chips with hyper bandwidth can be interconnected with a flat switching layer, and the diameter is only 2 ~ 4 inter-node hops. The network cost per injection/All-Reduce bandwidth of *RailX* is less than 10% of the Fat-Tree, and the cost per bisection/All-to-All bandwidth is less than 50% of the Fat-Tree. Specifically, only ~\$1.3B is required to interconnect 200K chips with 1.8TB bandwidth. *RailX* can also be used in the ML-as-a-service (MLaaS) scenario, where single or multiple training workloads with various shapes, scales, and parallelism strategies can be flexibly mapped, and failures can be worked around.

1 INTRODUCTION

In recent years, AI workloads have become increasingly large, growing much faster than the hardware [32, 42, 43, 59, 89]. To support hyper-scale *Large Language Model (LLM)* training workloads, hyper-scale infrastructures are required [31, 32,

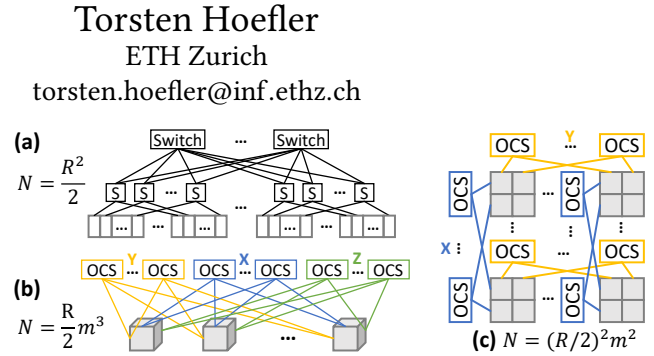


Figure 1: Scalability comparison of different topologies. R is the switch radix, and m is the local mesh/cube scale. (a) Two-level rail-optimized Fat-Tree; (b) OCS-based 3D-Torus; (c) RailX.

57, 95, 125]; however, traditional network architecture is neither scalable nor cost-effective enough.

Fat-tree-based topologies are widely used in existing data-centers; however, they are extremely expensive to provide sufficient bandwidth [13, 42, 43, 48], especially at hyper-scale. As shown in Figure 1(a), the *rail-optimized* network topology [72, 85, 91, 95, 116], collaborating with high-bandwidth scale-up networks (e.g., *NVLink* network [53, 111]), reduces the number of spine/core switches while maintaining performance [84]. However, the bandwidth and scalability are still limited by the high-radix packet switch and the scale-up network, both of which are expensive to further scale. Besides, multi-stage switching also introduces significant energy and latency overhead [46, 60, 92, 114], potentially preventing system scaling.

Direct networks, though they do not require high-radix switches, also face the scalability challenge. The Torus topology naturally fits the traffic of traditional AI workloads [45, 58] with data/tensor/pipeline parallelism (DP/TP/PP) [51, 57, 82, 105]. However, with the parameter/activation size scaling, more parallel strategies, including sequence parallelism (SP) [64], expert parallelism (EP) for mixture-of-experts (MOE) models [22, 27–29, 35, 55, 69, 97, 99] and

*Corresponding Author

context parallelism (CP) for long sequences [54, 71, 86], are adopted and combined, making mapping on Torus complex. Moreover, the diameter of regular/twisted Torus networks is large, and the bisection bandwidth is insufficient for all-to-all traffic of MOE and ranking models [14, 41, 83]. Furthermore, direct networks face flexibility and reliability challenges; thus, as shown in Figure 1(b), *Google TPUv4* cluster introduces optical circuit switches (OCSes) to reconfigure the interconnection [125]. However, the centralized optical switching layer limits the network scalability by the OCS port count (*i.e.*, no more than 64 cubes by using 128-port OCSes [70]).

There are a few other academic topologies, including *HammingMesh* [48], *BML* [115], *TopoOpt* [117], *SiP-ML* [62], and *Rail-only* [116], designed for AI training workloads. However, they do not take the latest hyper-scale workloads with high-dimensional hybrid parallelism (especially expert parallelism) into account, and their scalability is still limited by the radix of packet/circuit switches (specifically, hard to scale to >100K chips with flat switching layer). Therefore, we are motivated to design a more scalable network architecture for modern hyper-scale LLM training workloads.

In this paper, we present the *RailX* network architecture, where “X” indicates the crossing of rails. As shown in Figure 1(c), locally, chips within a node are directly interconnected by a high-bandwidth 2D-mesh, and the row/column rail ports of each node are connected to row/column circuit switches separately. By configuring the circuit switches, different row/column rails are interconnected into separate rings; simultaneously, nodes are interconnected into low-diameter topologies, including *HyperX* and *Dragonfly*. The major contributions of this paper can be summarized as follows:

- *RailX* fully utilizes advanced packaging/integration technologies and circuit switching, achieving ultra-high scalability and cost-effectiveness. Specifically, more than 100K chips can be interconnected with a flat (single-tier) 128-port circuit switching layer, and the typical diameter is only 2 ~ 4 inter-node hops. The network cost per injection/All-Reduce bandwidth of *RailX* is less than 10% of the Fat-Tree, and the cost per bisection/All-to-All bandwidth is less than 50% of the Fat-Tree.
- We propose the *Rail-Ring-based All-to-All* interconnection method based on *Hamiltonian Decomposition* theory [110] to construct an all-to-all topology from separate rings, achieving efficient All-Reduce and All-to-All communication simultaneously.
- We propose point-to-point routing and hierarchical collective algorithms to fully utilize local high-bandwidth

and low-latency links, achieving better All-Reduce performance than traditional ring-collective algorithms on Torus and HammingMesh.

- We also introduce the *Dimension Splitting* method to flexibly adjust the number of topology dimensions and the bandwidth/scale of each dimension, facilitating the mapping of diverse LLM training workloads with various types, shapes, scales, and parallelism (TP, CP, EP, DP, PP) strategies. In addition, *RailX* can be used in MLaaS scenarios, where single or multiple training workloads can be flexibly mapped and scheduled, and failures can be worked around.

2 CHALLENGES AND MOTIVATIONS

2.1 Advances in Hardware Technologies

In recent years, hardware technologies have made significant progress, promising to inspire new network architectures. Advanced integration technologies such as *Panel-Level Packaging* and *System-on-Wafer* allow many chips to be integrated into a single package [20, 30, 61, 68, 118], and high-speed interfaces provide high-bandwidth, low-power, and low-latency connectivity between chips [4, 106, 112, 119]. As shown in Table 1, the *UCIe* die-to-die interface provide 1317GBps/mm shoreline bandwidth density (1350GBps/mm² area density) within the package [4], much larger and cheaper than any traditional inter-chip interfaces. The latency and power consumption of such on-package interfaces are also much lower. At the same time, the *Co-Packaged Optics (CPO)* technology [76, 80] also significantly increases the off-package bandwidth density up to 128GBps/mm (32 400G ports per chip edge) [34, 78] and eliminates separate optical modules.

Interface	SerDes	UCIe
Physical Medium	Fiber/Copper Cable	RDL/Substrate
Density (GBps/mm)	128	1317
Latency (ns)	100 + ToF	2
Energy (pj/bit)	> 5	< 1
Channel Reach	> 10 m	< 25 mm

Table 1: Chip-to-chip interfaces [1, 4, 24, 34, 39, 78, 100]

However, there are also challenges in utilizing these technologies. Firstly, the wire density is high, and the connection distance is short; therefore, placement and wiring are challenging. Only flat topologies such as 2D-mesh and HexaMesh [52] are feasible within the package [16, 50, 90]. At the same time, there is a significant gap between on-package and off-package bandwidth. As a result, when scaling out

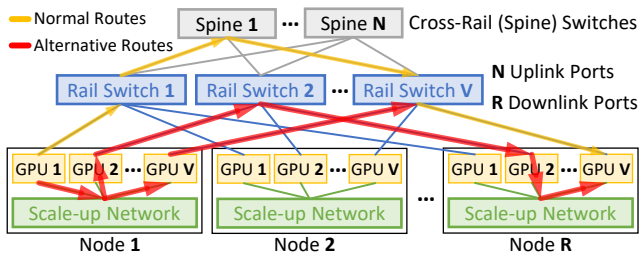


Figure 2: Rail-optimized Fat-Tree. The i -th GPU in each node is connected to the i -th rail switch.

packages into large system-level networks [109], the mismatched bandwidth can lead to low utilization. Besides, mapping highly parallelized AI training workloads on such networks is also challenging.

2.2 Challenges of Existing Networks for AI

2.2.1 Fat-Tree is expensive. In existing architectures, processors within a node are locally interconnected by a high-bandwidth low-latency Fat-Tree (e.g., NVLink network) [19, 33, 53]. As shown in Figure 2, in a rail-optimized Fat-Tree, the NIC/GPU- i of each node is connected to the same rail switch i ($i = 1, \dots, V$, where V is the number of GPUs per node). With proper mapping, most communication does not need to go through the cross-rail switches; thus, the traffic imbalance and the cost of the network (number of cross-rail switches) are reduced [116]. For massive cross-rail communication (e.g., all-to-all communication conducted by MOE and ranking models), local networks can be utilized to provide bandwidth among different rails [84, 97, 123]. As the example shown in Figure 2, messages from Node-1-GPU-1 can be sent to Node-1-GPU- V through the local network first, then to Node- R -GPU- V without going through the cross-rail switches.

Though the rail-optimized Fat-Tree is more cost-effective than the traditional Fat-Tree, the scalability challenge is still critical. Using rail switches with R downlink ports and nodes with V GPUs, a rail-optimized segment can only support $R \times V$ GPUs. The latest *Alibaba HPN* achieves 400 Gb/s bandwidth among 15K GPUs by using 360 51.2T switches [95]. At the same time, 7.5K NVLink switches are required to provide 400 ~ 900 GB/s local bandwidth. To further scale and increase the bandwidth, both the scale-out (Ethernet) and scale-up (NVLink) networks are expensive. For example, on the one hand, the GB200 NVL72 node (cabinet) has an average sale price of \$3M while 36 separate *GB200 Superchips* have a total price of \$2.16M [122]; that is to say, the scale-up network accounts for about 30% of the GPU node cost. On the other hand, to further interconnect the NVL72 node with 800G-per-GPU NIC in a 3-tier Fat-Tree, $72 \times 5 \times 800$ G switching bandwidth and $72 \times 3 \times 800$ G-links are required per node. If the prices of a 51.2T switch and an optical cable with transceivers are estimated at \$40K [81] and \$2K [6, 42, 43],

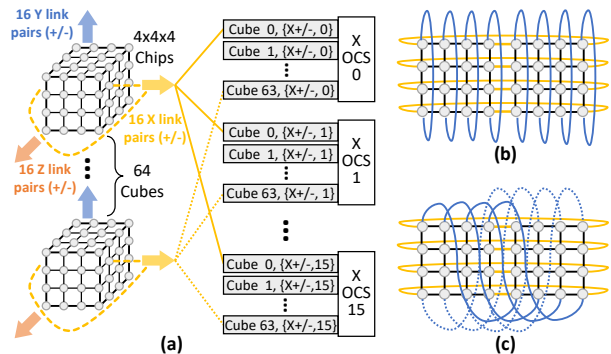


Figure 3: TPUv4 network architecture. (a) Each cube contributes two ports from opposite sides to each optical switch. (b) Regular Torus. (c) Twisted Torus.

the scale-out network introduces extra 21.9% cost. Besides, the energy ($> 10\text{W/Tbps/hop}$ [2], additional one fifth of the computing power [42]) and latency ($> 200\text{ns/hop}$ [60]) overhead of multi-layer switching are also significant. In summary, packet-switch-based Fat-Tree is too expensive to provide sufficient bandwidth at hyper scales.

2.2.2 Direct topologies have limited bisection bandwidth and flexibility. AI training workloads with the three typical parallelism strategies (tensor, data, and pipeline) introduce 3D-shape communication patterns; therefore, Torus topology provides optimal ring-collective performance for traditional AI workloads without using expensive packet switches [58]. As shown in Figure 3, for usability and reliability purposes, the *Google TPUv4* cluster introduces cheaper optical circuit switches to reconfigure interconnection among multiple 3D-cubes [125]. As a result, different shapes of regular/twisted 3D-Torus can be constructed for different workloads, and machine/chip/link failures can be worked around.

Though the Torus topology is cost-effective, it still faces scalability challenges. With the increase of model/data size, more parallel strategies, including expert parallelism with all-to-all traffic [69, 97, 99] and sequence/context parallelism [54, 71, 86], are adopted and combined [29, 32, 124]. As shown in Figure 4, a high-dimensional parallelism strategy is introduced for hyper-scale LLM training workloads. At the same time, attention and FFN (expert) layers adopt heterogeneous parallelism strategies due to the expert parallelism with all-to-all traffic (also see Figure 12 in § 5) [29, 97, 123]. The communication scope, volume, and frequency of different parallelisms are significantly different (e.g., TP usually introduces higher bandwidth requirement than DP [32, 116] and is hard to overlap with computation), but the dimension and bandwidth of the Tours topology is fixed and uniform. Therefore, mapping heterogeneous high-dimensional parallelism on Torus topologies is complex and inefficient.

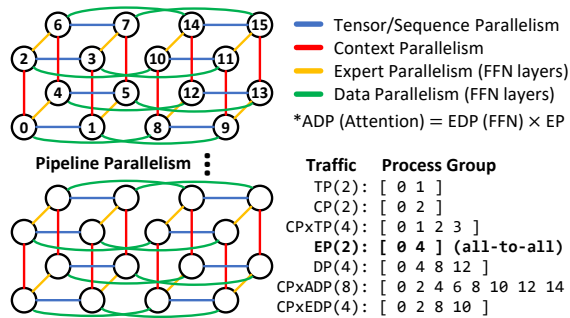


Figure 4: High-dimensional (TP, CP, EP, DP, PP) heterogeneous parallelism for hyper-scale LLM training.

At the same time, the diameter of the Torus topology is large, and the bisection bandwidth is insufficient for all-to-all communication, which is essential for MOE and ranking models and also appears in context parallelism [54]. As shown in Figure 3(c), to improve all-to-all performance, *TPUv4* network adopts the twisted Torus, which crosswise connects rows/columns (over a $2n \times n$ mesh, connect $(2n-1, y)$ to $(0, y)$ and $(x, n-1)$ to $((x+n) \% 2n, 0)$), thus improving bisection bandwidth by no more than two times [14]. However, the twisted connection requires different cube rows/columns to be connected to the same OCSes, which constrains the network scale N by the OCS radix R ($N = R/2$) but only brings limited benefits ($< 2 \times$ bisection bandwidth improvement). In addition, ring-collective on Torus cannot utilize the potential high-bandwidth benefits offered by intra-node direct connectivity.

3 RAILX ARCHITECTURE

3.1 Rail-Ring-based Interconnection

To address the challenges of traditional topologies, a new network architecture is motivated. One idea is inspired by the *Hamiltonian Decomposition of Complete Graphs* [110] that *the edges of the complete directed graph of k ($\neq 4, 6$) vertices can be partitioned into $k-1$ directed Hamiltonian cycles* (construction is shown in § A.1). As shown in Figure 5(a), a node has four rails (two $+/-$ ports per rail), and all inter-node links only connect the same rails. As shown in Figure 5(b), each rail forms a ring connecting all nodes in a different order. Consequently, five nodes form an all-to-all topology, and any two nodes are directly connected on two different rail rings (e.g., node-0 and node-1 are connected on rail-0 and rail-3). The formalized description of the *rail-ring-based all-to-all interconnection* is given in Lemma 3.1.

LEMMA 3.1. *Given a node with $k-1$ rails (each rail has $+/-$ two ports), the all-to-all topology of k ($\neq 4, 6$, only two exceptions) nodes can be constructed from $k-1$ rail-based Hamiltonian rings. Any two nodes (A, B) are directly connected on two different rails r_a and r_b : $A+ \xleftrightarrow{r_a} B-$ and $A- \xleftrightarrow{r_b} B+$.*

It is evident that such *all-to-all* interconnection has a shorter diameter and better bisection bandwidth than Torus; however, the max all-to-all scale is limited by the number of rails (ports).

Another idea is motivated by the *Interface Grouping* [38], which splits ports into different groups to adjust the number of logical dimensions and the bandwidth per dimension. As shown in Figure 5(c), four rails can be divided into two separate rail groups, forming a 2D all-to-all (HyperX [9]) topology with 3×3 nodes. A node with n rails can be interconnected into a k -D hyper-X topology with $(\frac{n}{k} + 1)^k$ nodes. It is also possible to let different rail groups have different numbers of rails and different interconnections. In this way, not only can the topology and bandwidth be flexibly adjusted, but the scalability is also improved.

3.2 Physical Architecture

The following symbols are used in the description:

Basically, *RailX* is a flat optical-circuit-switched network consisting of three physical levels: chip, node, and system. As shown in Figure 6(a), each chip is a processor/accelerator, and the original IO interfaces are high-density but short-reach (e.g., UCIe [4]). $m \times m$ chips within a node are directly interconnected through these high-bandwidth links, forming a 2D-mesh topology. All the interfaces at the edges are converted by IO chiplets/modules to long-reach optical ports for upper-level interconnection [15, 34, 49, 78]. If a chip has

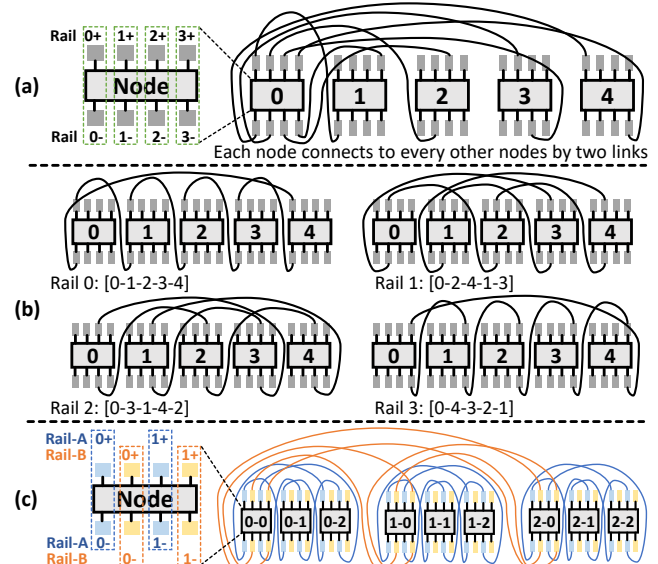


Figure 5: Rail-ring-based interconnection. (a) Each node is connected to every other node (b) 4 rails are interconnected into rings separately with different orders. (c) Four rails are divided into two separate rail groups, forming a 2D-HyperX (2D all-to-all) topology with 3×3 nodes.

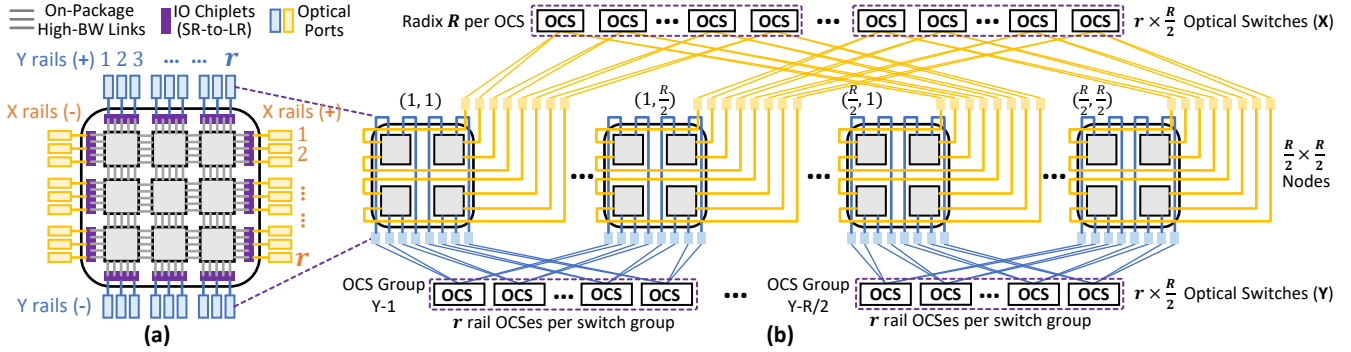


Figure 6: RailX physical architecture. (a) Chips within a node are connected into a 2D-mesh topology by high-bandwidth, low-latency direct links (e.g., UCIE [4] and UALink [108]). The short-reach interfaces at the edges are converted to long-reach optical ports for inter-node interconnection. (b) Nodes are connected to optical switches in a 2D organization ($\frac{R}{2} \times \frac{R}{2}$): different rows and columns of nodes are connected to different X/Y OCS groups ($r = mn$ OCSes per each group), and X/Y ports with the same rail-ID are connected to the same X/Y switch.

$m \times m$	The scale of the 2D-mesh of chip in a node
n	The number of off-package ports per chip edge
r	The number of rails per dimension (X/Y), $r = mn$
k	The multiple of on-package bandwidth over off-package bandwidth
R	The radix (port number) of the optical circuit switch
N	The total number of chips
B_c	Bisection bandwidth (TX + RX)
H_i, H_o	Internal direct hop and external optical hop

n ports at each edge, an entire node has $r = mn$ ports at each edge, and each pair of ports (+/−) for each row and column is called a rail. Advanced packaging technologies are optimal but not essential as long as the intra-node direct connectivity provides cheaper and higher bandwidth (e.g., NVLink and UALink [108]) than inter-node long-distance links.

As shown in Figure 6(b), all nodes in the system are connected to high-radix circuit switches in a 2D organization: X-rail a and Y-rail b of node (i, j) are connected to X-OCS (j, a) and Y-OCS (i, b) , respectively ($a, b \in [1, r], i, j \in [1, \frac{R}{2}]$). In other words, each node row and node column of the total $\frac{R}{2} \times \frac{R}{2}$ nodes are connected to one OCS group (r switches), and ports with the same rail-ID are connected to the same switch.

The physical architecture of RailX is a circuit-switched *HammingMesh* [48] and is similar to *TPUv4* but has two major differences. 1) **Chips are locally connected into a higher-bandwidth 2D-mesh rather than a uniform-bandwidth mesh or cube.** The short-reach direct connectivity can provide much higher and cheaper bandwidth with lower latency and energy consumption, which is not fully utilized by *HammingMesh* and *TPUv4*. Besides, the 2D-mesh with abundant bisection bandwidth is utilized as a high-bandwidth

switch [16, 36]; thus, low-diameter topologies can be constructed without introducing extra packet switches. In addition, the high-bandwidth 2D-mesh is regarded as a new hierarchy that facilitates more flexible mapping of training workloads with mixed and heterogeneous parallelism strategies, which will be further illustrated in § 3.3.4, 4.2, and 5.

2) **The nodes in RailX are connected to OCSes in a 2D organization rather than the centralized switching layer.** One advantage of *TPUv4* jointly connecting all cubes is to support the twisted Torus topology, which has a better bisection bandwidth. However, we have a better solution to provide a much higher bisection bandwidth; therefore, twisted Torus is not necessary so that we can interconnect different rows and columns separately to achieve high scalability. The total number of chips (N) and optical circuit switches (N_s) in RailX is:

$$\begin{cases} N = \left(\frac{R}{2}\right)^2 m^2, \\ N_s = rR. \end{cases} \quad (1)$$

With existing hardware technologies, the scale of RailX can be more than 100K chips ($R = 128$ [70] and $m = 5$ [109], then $N = 102400$). Even with normal PCB-level integration, the scale can still be more than 100K chips with higher-radix optical switches (e.g., $R = 320$ [3, 91] and $m = 2$). In comparison, the *TPUv4* pod (OCS-based 3D-Torus) can only support as many as $N_{TPUv4} = \frac{R}{2} m^3$ chips, limited by the 1D centralized switching layer.

3.3 Topology Configuration

Similar to *TPUv4*, the circuit switches are configured at the beginning of a large training job, and on-chip routers (low-radix packet switches) are used for routing under each specific configuration. Therefore, the switching latency, which is the most significant disadvantage of optical circuit switches,

is negligible. More fine-grained and dynamic reconfiguration (e.g., reconfiguration during each iteration) is also possible, which is briefly introduced in § 5.2.

By configuring optical switches, different logical topologies, including Torus, Draonglfy [36, 63], and HyperX [9], can be constructed and combined based on the interconnection method described in § 3.1. The comparison of three base topologies is summarized in Table 2. Topology configurations are according to the workload, trading off among scalability, diameter, and bisection bandwidth. Besides these three based topologies, other existing topology optimization methods based on optical switching, such as *TopoOpt* [117], can also be utilized.

Topology	Torus	HyperX	Dragonfly
Scalability	$(\frac{R}{2})^2 m^2$	$(r+1)^2 m^2$	$(r+1)\frac{R}{2}m^2$
Diameter (H_o)	R	2	3
Bisection BW	$\frac{16n}{Rm}$	$\frac{2n}{m}$	$\frac{2n}{m}$

Table 2: Comparison of different 2D topologies

3.3.1 2D-Torus. The Torus topology can be naturally constructed by connecting the X-rails and Y-rails into parallel rings, just like the *TPUv4*. Since Torus only connects adjacent nodes, all nodes in the system can be connected into an entire $\frac{R}{2}m \times \frac{R}{2}m$ 2D-Torus. Though Torus provides optimal all-reduce bandwidth, the diameter is up to $R(H_o + (m-1)H_i)$, and the theoretical upper-bound throughput [23] for all-to-all communication is only

$$T_{\text{Torus}} = \frac{2B_c}{N} = \frac{4Rmn}{(\frac{R}{2})^2 m^2} = \frac{16n}{Rm} \quad (2)$$

per chip, significantly decreasing with the scale. Therefore, 2D-Torus is not suitable for complex workloads with non-ring-collective traffic (e.g., MOE model with all-to-all traffic in the EP dimension).

The workload mapping and collective algorithms of *RailX-Torus* are different from the regular Torus, where each parallelism is aligned with dimension scales. Take the *TPUv4* Pod slice with topology $8 \times 16 \times 16$ as an example, the tensor parallelism is 8-way mapped on the 8-scale dimension or 16-way mapped on a 16-scale dimension [45]. As for the *RailX-Torus*, the high-bandwidth 2D-mesh can be utilized to apply hierarchical collectives [18] or as a high-bandwidth local dimension. Details will be illustrated in § 3.3.4 and 4.2.

3.3.2 2D-HyperX. The regular HyperX is a direct network of S^D switches where switches belonging to the same dimension are fully connected [9]. For example, in an $S \times S$ HyperX, S switches in each row and each column are all-to-all connected. Compared with the Torus, HyperX has a

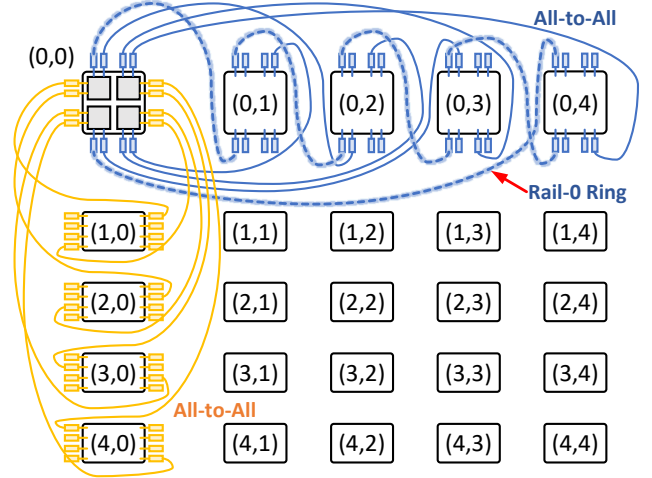


Figure 7: 2D-HyperX configuration of 25 nodes. 4 X-rails and 4 Y-rails are separately configured into ring-based all-to-all (as shown in Figure 5).

much shorter diameter (equals to the dimension number D) and a much higher bisection bandwidth.

Based on the interconnection method described in § 3.1, “switch-less” HyperX can be constructed in the *RailX*. As shown in Figure 7, the X-rails and Y-rails are separately interconnected into rail-ring-based all-to-all (two direct links between every node pair in every dimension), forming a $(r+1) \times (r+1)$ 2D-HyperX. Different from the regular HyperX, there are no extra high-radix packet switches in the *RailX-HyperX*, and there are two direct links between every node pair in every dimension.

The maximum scale of the *RailX-2D-HyperX* topology is $(r+1)^2 m^2$, limited by the rail number per node. If r is large enough (i.e., $r+1 = \frac{R}{2}$), the entire system can be configured into a single 2D-HyperX. With advanced CPO technologies (e.g., Broadcom achieves 32 optical ports per chip edge [78]), the rail number of a node can be even larger than the optical switch; thus there can be more physical channels between all-to-all pairs. All-to-all interconnection of $\frac{r}{a} + 1$ nodes can be constructed by connecting every node pair with $2a$ rails.

For the maximum size, the bisection bandwidth for each HyperX row/column is up to $4(\frac{r+1}{2})^2$. Thus, the bisection throughput for all-to-all communication is

$$T_{\text{HyperX}} = \frac{2 \times (r+1) \times 4(\frac{r+1}{2})^2}{(r+1)^2 m^2} \approx \frac{2n}{m} \quad (3)$$

per chip, more scalable than the 2D-Torus. The evaluation results are shown in § 6.3. Besides, diameter of the 2D-HyperX is only $2H_o + (5m-6)H_i$ (details are shown in § 4.1), also much smaller than 2D-Torus.

3.3.3 Dragonfly. The regular Dragonfly is another low-diameter topology where switches are locally fully connected

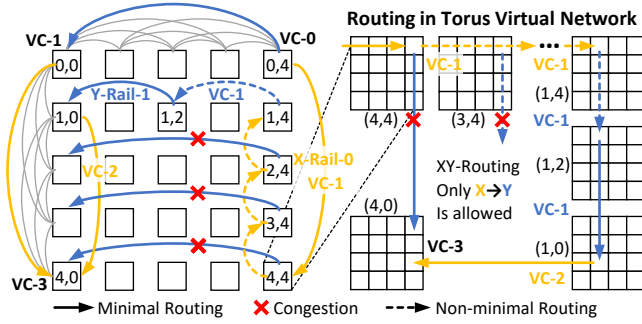


Figure 10: Minimal and non-minimal adaptive routing from (0, 4) to (4, 0) on 2D-HyperX.

the intra-node bandwidth of the 2D-mesh should be at least twice the inter-node bandwidth. According to our evaluations in § 6.3, 2 ~ 4× higher bandwidth is sufficient to provide non-blocking switching capability, which is easy to achieve by using short-reach direct links.

4 COMMUNICATION ALGORITHMS

Due to the good features of rail-ring-based all-to-all interconnection, many existing algorithms can be borrowed from Torus, Dragonfly, HyperX, and HammingMesh topologies. The major difference is the high-bandwidth local 2D-mesh, which brings benefits but also introduces routing challenges.

4.1 Point-to-Point Routing

4.1.1 Minimal-Routing. Minimal routing algorithms on RailX-based HyperX are similar to traditional HyperX [9, 77], but extra routing hops are required over the local 2D-mesh. Two minimal routes from source node (0, 4) to destination node (4, 0) are drawn in Figure 10: messages traverse to node (0, 0) or (4, 4) first and then to node (4, 0). Since nodes are connected by two links on both mesh sides (see Figure 7), if we always choose the nearest inter-node link when routing on 2D-mesh, a packet travels at most $(\frac{m}{2} - 1) + (m - 1)$ internal hops at each non-destination node and at most $2(m - 1)$ internal hops at the destination node. Therefore, the diameter of the 2D-HyperX is no more than $2H_o + (5m - 6)H_i$. The on-mesh routing algorithm can be deterministic or adaptive (e.g., dimension-order or north-last [44]) based on one single virtual channel (VC). As long as we increase VC at each node hop along the routes, any deterministic or adaptive minimal routing algorithm on HyperX is deadlock-free. A specific example is given in Algorithm 1, where (X, Y) and (x, y) are the node coordinate in 2D-HyperX and the chip coordinate in 2D-mesh, respectively. For other topology configurations, similar methods can be applied, and the required VC number for deadlock-free minimal routing equals the inter-node diameter (d_o) plus one.

Algorithm 1 DETERMINISTIC MINIMAL ROUTING

Input: Current chip coordinate: (X_c, Y_c, x_c, y_c) ;
Destination chip coordinate: (X_d, Y_d, x_d, y_d) .

- 1: **if** $X_c = X_d \ \& \ Y_c = Y_d$ **then** // Arriving Destination
- 2: ROUTING-ON-MESH(x_c, y_c, x_d, y_d) by VC-2
- 3: **else if** $X_c \neq X_d$ **then** // X-Rail-First
- 4: $(x', y') \leftarrow$ the nearest chip links to (X_d, Y_c)
- 5: **if** $(x_c, y_c) = (x', y')$ **then**
- 6: X-RAIL(X_c, X_d) by VC-1
- 7: **else if** $(x_c, y_c) \neq (x', y')$ **then**
- 8: ROUTING-ON-MESH(x_c, y_c, x', y') by VC-0
- 9: **end if**
- 10: **else if** $X_c = X_d \ \& \ Y_c \neq Y_d$ **then**
- 11: $(x'', y'') \leftarrow$ the nearest chip links to (X_d, Y_d)
- 12: **if** $(x_c, y_c) = (x'', y'')$ **then**
- 13: Y-RAIL(Y_c, Y_d) by VC-2
- 14: **else if** $(x_c, y_c) \neq (x'', y'')$ **then**
- 15: ROUTING-ON-MESH(x_c, y_c, x'', y'') by VC-1
- 16: **end if**
- 17: **end if**

4.1.2 Non-minimal Adaptive Routing. Minimal routing is not always optimal when traffic is unbalanced (e.g., all-to-all traffic of MOE models [17]); therefore, non-minimal adaptive routing algorithms are necessary [63, 77]. For any routing algorithm, we can always adopt the same method as the minimal routing: increasing VC at each node hop along the routes. However, the required VC number is as many as the length of the longest route.

Due to the good features of rail-ring-based interconnection (2D-rings), we can leverage the Torus routing algorithm to achieve deadlock-free non-minimal routing on RailX with fewer VCs. Previous studies have shown that only two VCs are required for deadlock-free XY routing on 2D-Torus [23], and only one single VC is sufficient if using *Bubble* flow-control techniques [74, 94]. The basic idea is to fully utilize each VC by using XY-routing-based Torus virtual networks where packets are routed along the X-rail and then the Y-rail. As shown in Figure 10, packets use VC-0 at the source node (0, 4) and then increase to VC-1 at the intermediate node (4, 4). If the direct channel between (4, 4) and (4, 0) is congested, adaptive misrouting can be performed. As long as the packet follows the XY-routing algorithm on Torus, it can be freely routed in the VC-1 network. In the figure, the packet is routed to node (1, 4) along the X-rail-0 and then routed to node (1, 0) along the Y-rail-1. Once the packet wants to change to X-rails, which violates the XY-routing algorithm, it must increase to VC-2. Finally, it is routed to the destination at node (4, 0) through VC-3. With this method, we combine limited times ($a > d_o$) of free routing and infinite times of Torus routing to achieve deadlock-free non-minimal routing on RailX with a limited number ($a + 1$) of VCs.

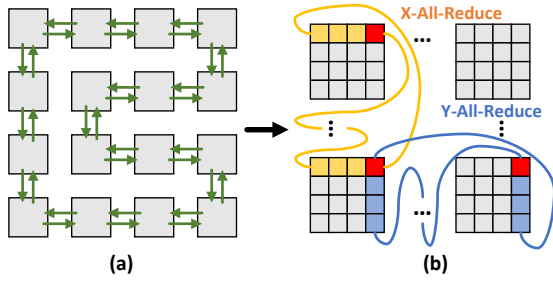


Figure 11: Hierarchical All-Reduce algorithm on RailX. (a) Bidirectional-ring-based All-Reduce on local 2D-mesh. (b) 2D-ring-based All-Reduce.

4.2 Collective Communication Algorithm

For AI training workloads, *All-Reduce* algorithms, which equals to one *Reduce-Scatter* followed by one *All-Gather*, are essential. Due to the rail-ring-based interconnection, existing collective algorithms on Torus such as *Ring* [12] and *Swing* [101] can be directly applied to RailX topology. The communication time of the bidirectional-ring-based *Reduce-scatter* and *All-gather* algorithm can be estimated as [18]

$$T_R(p, V, B) = (p - 1)\alpha + \frac{p - 1}{p} \frac{V}{2B}, \quad (6)$$

where p is the number of processors, α is the step (hop) latency, V is the data volume, and B is the bandwidth.

The 2D-ring-based algorithm on the RailX network splits data into two chunks and simultaneously executes the hierarchical algorithm [18] in both X and Y dimensions [48, 98]. Therefore, the communication time of the 2D-ring-based All-Reduce algorithm on the $m^2 \times p \times p$ RailX (2D-Torus or 2D-HyperX) can be estimated as ¹

$$T_{2D\text{-Ring}} = 2 \left[T_R \left(mp, \frac{V}{2}, nB \right) + T_R \left(mp, \frac{V}{2mp}, nB \right) \right] \approx 4mp\alpha + \frac{V}{2nB}, \quad (7)$$

where α is the inter-node optical hop latency, nB is the total bandwidth per chip edge. Though many of the hops along the ring are on-package hops, the total communication time is limited by the slowest hop, *i.e.*, the inter-node hop.

To fully leverage the high on-package bandwidth in RailX, we present a hierarchical All-Reduce algorithm. As shown in Figure 11(a), we can first perform local All-Reduce algorithms [66, 75] (*e.g.*, bidirectional ring[67]) over the high-bandwidth 2D-mesh. Then, as shown in Figure 11(b), global All-Reduce is performed. All the chips with the same local rank ID are still connected by the same X/Y-rail, and the inter-node bandwidth is shared by m chips (local ranks) along the rail. The communication time of the hierarchical All-Reduce

¹ \approx : we omit lower order term $o(p)$ and on-package hop latency

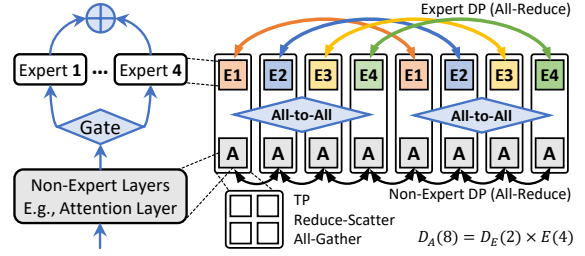


Figure 12: Expert parallelism.

algorithm on the $m^2 \times p \times p$ RailX network is estimated as

$$T_{\text{RailX}} \approx 2 \times \frac{V}{2knB} + \left(4p\alpha + \frac{V/m^2}{2nB/m} \right) = 4p\alpha + \left(\frac{2}{k} + \frac{1}{m} \right) \frac{V}{2nB}, \quad (8)$$

where k is the multiple of on-package bandwidth (in local 2D-mesh) over off-package bandwidth. We can see that the on-package bandwidth is utilized, and only p rather than mp inter-node steps are required. Typically, as long as $k > 2$, our hierarchical algorithm on RailX achieves better global All-Reduce performance than the traditional 2D-ring-based algorithms. The evaluation results are shown in § 6.4. We can also utilize the all-to-all interconnection in HyperX configuration to achieve a lower-latency All-Reduce algorithm, whose latency does not increase with the scale p . Limited by the space, it is shown in § A.2.

As for specific mapping of training workloads, if the tensor parallelism is mapped on the high-bandwidth 2D-mesh, which is the typical mapping, the communication of other parallelisms (*e.g.*, data parallelism) is among chips in different nodes with same local rank ID, and the inter-node bandwidth is shared by m chips. Therefore, the communication time of 1D (among p nodes) and 2D (among $p \times p$ nodes) node-level All-Reduce algorithm is estimated as

$$T_{1D} \approx 2p\alpha + \frac{V}{nB/m}, \quad T_{2D} \approx 4p\alpha + \frac{V}{2nB/m}. \quad (9)$$

As mentioned in § 3.3.4, we split the rails of the two physical dimensions to construct high-dimensional logical topologies. Collective communication may be performed among multiple dimensions. For example, the communication of QKV layers (non-expert layers) data parallelism is among CP/EP/DP dimensions (see § 5 and § A.3 Table 4). Similar methods can be adopted for high-dimensional All-Reduce over high-dimensional topologies, and we denote the communication time by $T_{hD}(n_1, \dots, n_h)$, where $n_i \times B$ is the bandwidth of dimension i . Besides our algorithms, there are other fine-grained collective scheduling algorithms [73, 96, 98, 102, 120, 121] that can be applied.

5 MAPPING AND SCHEDULING

4D parallelism (TP, CP, PP, DP) is used to train the latest Llama 3 405B model [32]. On this basis, we consider a larger-scale model with the MOE structure and introduce the expert parallelism (EP) over the expert (FFN) layers [29, 53, 97, 107, 124]. For simplicity’s sake, we assume both the attention and FFN layers adopt the same TP, CP, and PP scale. Therefore, as shown in Figure 12, the DP scale of attention layers equals the total scale of DP and EP of FFN layers ($D_a = ED_e$). The order of parallelism dimensions is $[T, C, E, D_e, P]$, where the innermost tensor parallelism usually introduces the most massive communication traffic. One mapping example is illustrated in § 3.3.4, and the communication pattern and time of each parallelism are shown in § A.3 Table 4. Many existing scheduling methods, such as CASSINI [96], can be borrowed for mapping and scheduling on *RailX*. Limited by the space, this paper only focuses on the bandwidth allocation scheduling for the *Dimension Splitting* method.

5.1 Static Allocation

As discussed in § 3.3.4, we split the rails of each node into multiple dimensions according to the shape of workloads. The static allocation is to configure the network topology at the beginning of a training job and not reconfigure within training iterations, which is a common way with “slow-switching” OCSes [70, 117].

In practice, the factors affecting real efficiency are very complex. Besides the communication efficiency, the computation efficiency and the communication-computation overlap are also important. A highly generalized expression

$$T_{\text{Actual}} \approx T_{\text{Comp}} + \max \left\{ T_{\text{Comp}}^*, T_{\text{Comm}}^* \right\} + T_{\text{Comm}} \quad (10)$$

is used to estimate the total time, where $T_{\text{Comp}}/T_{\text{Comm}}$ is the computation/communication time that cannot be overlapped, $T_{\text{Comp}}^*/T_{\text{Comm}}^*$ is the time that can be overlapped. As the example shown in Figure 9, if we split the bandwidth for DP and PP ($n = n_d + n_p$), both of which can be overlapped, the actual total time we want to minimize is

$$\arg \min_{n_d, n_p} \left\{ \max \left(T_{\text{Comp}, d}^*, \frac{V_d}{2n_d B} \right) + \max \left(T_{\text{Comp}, p}^*, \frac{V_p}{2n_p B} \right) \right\}, \quad (11)$$

where, V is the data volume of each parallelism, and B is the bandwidth per each port.

During the entire training process, the mapping strategies and bandwidth allocation can still be adjusted. For example, in Llama 3 405B training, the context length gradually increases from 8K to 128K in six stages [32], and the context parallelism is introduced only for long context length. Therefore, the bandwidth allocation may also be adjusted when the parallelism and mapping change. However, such

adjustments are not frequent, so they are still regarded as static allocations. Exploration results are shown in § 6.5.

5.2 Dynamic Allocation

Based on static allocation, which splits the bandwidth of one physical dimension into two logical dimensions in a fixed way, we tend to map the highest and lowest communication to one dimension. *E.g.*, if the communication requirement is $EP > CP > DP > PP$, the optimal allocation is to map the EP and PP to one physical dimension and the CP and DP to the other physical dimension.

However, if the two communications are separated by other communication or computation, we can use circuit switching to allocate the bandwidth dynamically. As shown in Figure 13 (also shown in § A.4 Figure 21), CP and EP communications are non-overlapped. They are separated by the computation of attention input/output projection, the communication of SP/TP, and the pre/post-process of MOE layers [8, 86]. The time interval is about a few milliseconds for the small-scale model and can be longer for larger models. Therefore, it is possible to dynamically configure the circuit switch and allocate the bandwidth for CP and EP communications. As a result, both CP and EP communications can fully utilize the bandwidth of one entire physical dimension.

6 EVALUATION

6.1 Methodology

We use a cycle-based network simulator and a hardware-validated analytical model to evaluate *RailX*.

6.1.1 Analytical Model and Trace Synthesis. Due to the impracticality of collecting real traces from extreme-scale AI training workloads, we build a hardware-validated analytical model to give estimates of the computation and communication. To validate the analytical model, we run training workloads with small-scale hybrid parallelism on real hardware and collect the trace by using NVIDIA Nsight Systems [88]. Details are shown in § A.4. The computation time of larger tiles/blocks is estimated based on the computing FLOPS (multiples of FLOPS \times measured time of small tiles/blocks). The volume and scopes of major communication are directly extracted from the training framework and validated by the Nsight traces.

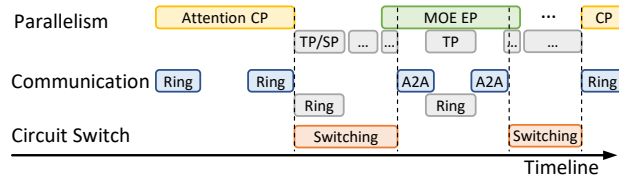


Figure 13: Circuit switching to allocate all bandwidth between context parallelism and expert parallelism.

6.1.2 Cycle-based Simulator. We build a cycle-based network simulator based on the CNSim framework [37], which supports fine-grained microarchitecture modeling and multithreading (also see § A.6), to evaluate the communication performance of *RailX*. To simplify and accelerate the simulation, we omit complex network protocols and use the ideal virtual cut-through router and the credit-based lossless flow control [23]. The bandwidth of the slowest link (inter-node link) in the network is normalized to 1 flit/cycle (e.g., 64 Gb/s bandwidth at 8B flit size and 1GHz frequency), and the on-chip/intra-node link bandwidth is k multiples. The default input buffer size per virtual channel of the router is 16 flits (i.e., maximum message size). The evaluated traffic patterns are synthesized by the hardware-validated analytical model. The inter-node latency is set to 10 cycles, while the intra-node latency is set to 1 cycle.

6.2 Cost Analysis

We compare the cost of several typical systems: 1) non-blocking/tapered Fat-Tree; 2) HammingMesh (HxaMesh with $a \times a$ boards) ; 3) 3D-Torus without OCS; 4) TPUv4 (OCS-based 3D-Torus); 5) 2D Fat-Tree (Rail-Only [116], see § A.8); 6) RailXaMesh. For a fair comparison, we assume all chips have 1.8TB/s (36×400G) off-package bandwidth; specifically, 36 rails for Fat-Tree, 18 rails for 2D Fat-Tree, 9 planes for HammingMesh, 6 ports per direction for 3D-Torus, and $n = 9$ rails per chip for RailX. Short-reach package/PCB-level connectivity is used for 2D-mesh; passive copper cables (PCCs) are used for 3D-cube (inter 2×2 mesh boards [58]); and active optical cables are used for inter-mesh/cube/switch connections. The cost is estimated based on the components, and we assume OCS has twice as many ports as electrical packet switches at the same cost [70, 91, 93, 113, 117]. A passive 400G copper cables costs \$250 [7], an 400G active optical transceiver (AOT) costs \$1000 [6, 42, 43], a 64-port 400G packet switch or a 128-port OCS costs \$35K [5]. The cost of short-reach package/PCB-level connectivity is neglected (included in chips). It should be noted that, with $n = 9$, $m = 7$ results in $r = 63$ to match the OCS radix $R/2 = 64$.

The results are shown in Table 3 (details are in § A.7 Table 6), where the upper part is evaluated at maximum or original scale, and the lower part is evaluated at uniform scale (~200K chips). The cost per injection bandwidth approximates the cost per All-Reduce bandwidth. Compared with Torus, RailX uses high-bandwidth 2D-mesh to eliminate all the copper cables and significantly improve the bisection bandwidth. Compared with the Fat-Tree, RailX achieves the same All-Reduce bandwidth at less than 10% cost. Compared with HammingMesh, which is the previous SOTA topology, RailX uses optical switching to reduce half of the cost while maintaining the throughput and improving the scalability.

Table 3: Scalability/cost comparison (packet/circuit switch radix is 64/128, details are in § A.7 Table 6).

Topology	Scale [#]	Cost [M\$]	Cost [/ Inject]	Glob. BW [% Inject]	Cost [/ GBW]
2-Tier FT	2048	415.9	1×	100	1×
1:3 Tap. FT	3072	395.7	0.65×	33.3	1.90×
1-FT Hx4Mesh	16384	375.6	0.11×	12.5	0.90×
1-FT Hx7Mesh	50176	657.2	0.06×	7.1	0.91×
TPUv4	4096	185.7	0.22×	4.2	5.52×
3D-Torus	4096	45.0	0.05×	4.2	1.46×
2D 1-FT	4096	375.6	0.45×	50	0.90×
RailX4Mesh	65536	751.1	0.06×	12.5	0.45×
RailX7Mesh	200704	1314.4	0.03×	7.1	0.45×
4-Tier FT	196608	83718	2.10×	100	2.10×
49:7:1 Tap. FT	200704	22052	0.54×	2.0	26.5×
2-FT Hx7Mesh	200704	5822	0.14×	7.1	2.01×

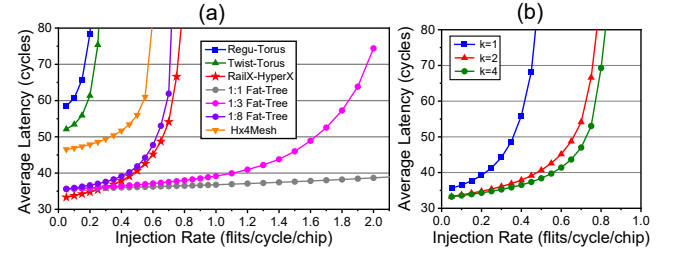


Figure 14: All-to-all performance. (a) Different topologies with 1.3K chips; (b) RailX with different intra-mesh bandwidth (k times the inter-node bandwidth).

6.3 All-to-All Performance

We simulate the all-to-all performance of *RailX-2D-HyperX* ($m = 4$, $n = 2$, $N = 1296$) and other topologies. All topologies have around 1.3K chips, and each chip has 8 ports (i.e., 8 flits/s/cycle/chip injection bandwidth). As shown in Figure 14(a), *RailX* achieves 0.8 flits/cycle/chip throughput, which is close to the theoretical maximum throughput of 1 flits/cycle/chip. Compared with all other topologies, *RailX* achieves the most cost-effective all-to-all throughput. Compared with HammingMesh, *RailX* adopts higher intra-mesh bandwidth and eliminates the packet switches, thus achieving higher actual throughput and lower latency.

As analyzed in § 3.3.5, the intra-mesh bandwidth is essential for *RailX* as the 2D-mesh is utilized as a virtual switch. We simulate the performance with different internal bandwidths. As shown in Figure 14(b), if the internal bandwidth is the same as the external bandwidth, the performance is poor because the 2D-mesh becomes the bottleneck. With 2× internal bandwidth, the performance is significantly improved and close to the theoretical maximum throughput. Higher internal bandwidths do not bring significant improvement, as the external bandwidth becomes the bottleneck.

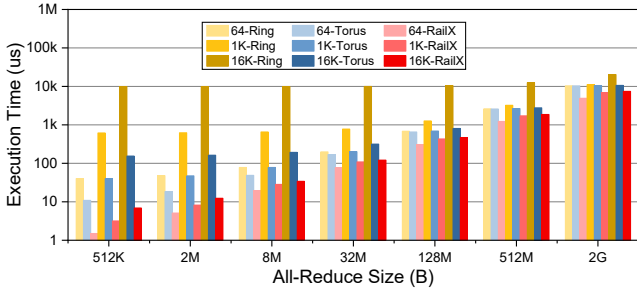


Figure 15: All-Reduce performance.

6.4 All-Reduce Performance

We also evaluate the All-Reduce performance of *RailX*. 1D-ring, 2D-Torus [48], and hierarchical-2D-Torus algorithm presented in § 4.2 are evaluated with different scales and sizes. We assume each chip has four ports (double bandwidth for the 1D-ring), the external bandwidth is set to 100GB/s per port, and the internal bandwidth is set to 400GB/s per port (*i.e.*, 200GB/s for 1D-ring All-Reduce on 2D-mesh). The latency is set to 300ns per external hop [101] and 10ns per internal hop.

As shown in Figure 15, the hierarchical-2D-Torus algorithm on *RailX* always achieves the best performance (shortest time to finish). For large-size All-Reduce, since all algorithms are near bandwidth-optimal, they achieve similar performance. For small-size All-Reduce, the 1D-ring algorithm has the worst performance, and the hierarchical-2D-Torus algorithm outperforms the 2D-Torus algorithm, especially at hyper-scale.

6.5 Bandwidth Allocation Exploration

As discussed in § 5.1, the bandwidth of one physical dimension is allocated to two parallelism dimensions according to the communication volume and the overlap with computation. The results of allocation (10 ports in total) between DP and CP with different sequence lengths are shown in Figure 16, where the actual communication times under different allocation proportions are measured. For small-scale sequence length, the CP communication is relatively small; therefore, the optimal policy is to allocate more bandwidth to DP. As the sequence length increases, the CP communication rises; thus, we tend to allocate more bandwidth to CP. After considering the computation/communication overlap of DP, we are supposed to allocate even more bandwidth to CP. In summary, optical switching with the *dimension-splitting* method provides flexibility to adjust the bandwidth of each parallelism dimension for different configurations.

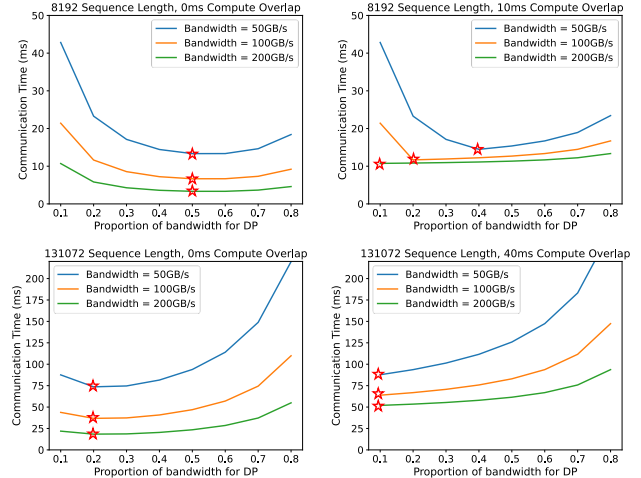


Figure 16: Different sequence length and computation-communication overlap introduce different bandwidth allocation strategies.

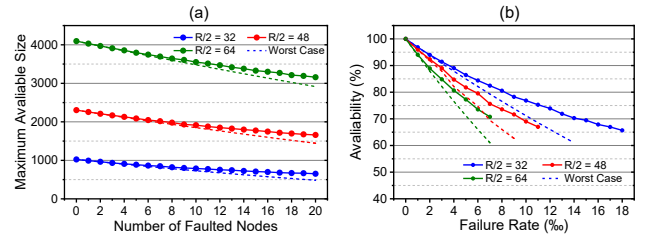


Figure 17: Availability of single allocation with OCS configurability. (a) Maximum size for a single job with faulted nodes; (b) Availability at failure rates.

6.6 Reliability and Availability

Similar to TPUv4 [125], *RailX* also gains reliability and availability benefits from bypassing failure nodes with OCS configurability. However, due to the 2D organization, a failure node will cause the row and the column to be disconnected, which is similar to the *HammingMesh* [48]. By using proper allocation policy, we can fully utilize all nodes (as shown in § A.5) in *ML-as-a-service* (*MLaaS*) scenario.

However, when using the entire system for one single job, there is no optimization room for utilizing disconnected nodes; therefore, the failure nodes will significantly affect availability. In the best case, all failure nodes are in the same row or column; we only lose one row or one column of nodes; in the worst case, the failure nodes (*e.g.*, 2a) are distributed in different rows and columns; as a result, the maximum allocation for single job is $(R/2 - a) \times (R/2 - a)$. For general cases, the maximum allocation is an NP-hard problem; however, since the failures are sparse, we can use a fast algorithm (shown in § A.5) to find the maximum allocation.

In evaluation, we randomly select nodes as failure nodes and calculate the maximum allocation for a single job. We use 100 random samples for each failure rate and calculate the

average. As shown in Figure 17(a), the maximum available size decreases linearly with the number of failure nodes, and the average size is significantly better than the worst case when the failure rate is high. As shown in Figure 17(b), with the same failure rate, the large-scale *RailX* has worse availability than the small-scale *RailX*. Considering a typical failure rate of 0.1% [125], the availability is always more than 90%, which is acceptable for large-scale training systems.

7 RELATED WORKS

HammingMesh also leverages local 2D-mesh networks, providing high All-Reduce bandwidth at a low cost [48]. From the topology perspective, *RailX* is a circuit-switched *HammingMesh* with higher local bandwidth inside the 2D-mesh. As a result, *RailX* achieves higher scalability and higher AllReduce throughput than *HammingMesh*. Limited by the space, more related works are shown in § A.8.

8 CONCLUSIONS

RailX is a novel network architecture optimized for large-scale LLM training systems. By utilizing advanced integration technologies (high-bandwidth 2D-mesh), 2D-organized circuit switches, and *rail-ring-based all-to-all* interconnection, *RailX* achieves higher scalability and cost-effectiveness than existing topologies. It provides extreme injection/All-Reduce bandwidth at hyper scales and very low cost (less than 10% compared with the Fat-Tree) while maintaining sufficient bisection/All-to-All bandwidth. *RailX* also demonstrates high flexibility in the MLaaS scenario. Circuit switching allows single or multiple jobs to be flexibly scheduled, and failure nodes can be easily worked around. With the *dimension-splitting* method, the number of topology dimensions and the bandwidth/scale of each dimension can be flexibly adjusted according to the workload.

REFERENCES

- [1] 2022. Common Electrical I/O (CEI) - Electrical and Jitter Interoperability Agreements for 6G+ Bps, 11G+ Bps, 25G+ Bps, 56G+ Bps and 112G+ Bps I/O. (Dec. 2022). www.oiforum.com/wp-content/uploads/OIF-CEI-5.1.pdf
- [2] 2024. Marvell Teralynx 51.2T Ethernet Switch Enters Volume Production for Global AI Cloud Deployments. <https://www.marvell.com/company/newsroom/marvell-teralynx-512t-ethernet-switch-enters-volume-production-for-global-ai-cloud-deployments.html>. (2024). <https://www.marvell.com/company/newsroom/marvell-teralynx-512t-ethernet-switch-enters-volume-production-for-global-ai-cloud-deployments.html>
- [3] 2024. Photonic Optical Circuit Switching | CALIENT Technologies. <https://www.calient.net/>. (2024). <https://www.calient.net/>
- [4] 2024. Universal Chiplet Interconnect Express (UCIe) Specification Revision 2.0. (Aug. 2024). <https://www.uciexpress.org/specifications>
- [5] 2025. Mellanox Quantum-2 QM9700 64-Port Non-Blocking Managed NDR 400Gb/s InfiniBand Switch - Part ID: MQM9700-NS2F - Switches - Colfax Direct. <https://www.colfaxdirect.com/store/pc/viewPrd.asp?idproduct=4162&idcategory=7>. (2025). <https://www.colfaxdirect.com/store/pc/viewPrd.asp?idproduct=4162&idcategory=7>
- [6] 2025. NVIDIA 800Gb/s, Twin-Port, OSFP Multimode SR8 Transceiver - Finned Top - Part ID: MMA4Z00-NS - Colfax Direct. <https://www.colfaxdirect.com/store/pc/viewPrd.asp?idproduct=4272&idcategory=0>. (2025). <https://www.colfaxdirect.com/store/pc/viewPrd.asp?idproduct=4272&idcategory=0>
- [7] 2025. NVIDIA Passive Copper Cable, IB Twin Port NDR 800Gb/s, OSFP, 0.5 Meter - Part ID: MCP4Y10-N00A - Colfax Direct. <https://www.colfaxdirect.com/store/pc/viewPrd.asp?idproduct=4166&idcategory=0>. (2025). <https://www.colfaxdirect.com/store/pc/viewPrd.asp?idproduct=4166&idcategory=0>
- [8] 2025. NVIDIA/Megatron-LM. NVIDIA Corporation. (Jan. 2025). <https://github.com/NVIDIA/Megatron-LM>
- [9] Jung Ho Ahn, Nathan Binkert, Al Davis, Moray McLaren, and Robert S. Schreiber. 2009. HyperX: Topology, Routing, and Packaging of Efficient Large-Scale Networks. In *Proceedings of the Conference on High Performance Computing Networking, Storage and Analysis*. ACM, Portland Oregon, 1–11. <https://doi.org/10.1145/1654059.1654101>
- [10] Joshua Ainslie, James Lee-Thorp, Michiel de Jong, Yury Zemlyanskiy, Federico Lebrón, and Sumit Sanghai. 2023. GQA: Training Generalized Multi-Query Transformer Models from Multi-Head Checkpoints. (Dec. 2023). <https://doi.org/10.48550/arXiv.2305.13245> arXiv:cs/2305.13245
- [11] Brian Alspach. 2008. The Wonderful Walecki Construction. 52 (2008), 7–20.
- [12] Andrew Gibiansky. 2017. *Bringing HPC Techniques to Deep Learning*. Technical Report. Baidu Research. <https://andrew.gibiansky.com/blog/machine-learning/baidu-allreduce/>
- [13] Luiz André Barroso, Urs Hölzle, and Ranganathan Parthasarathy. 2019. *The Datacenter as a Computer: Designing Warehouse-Scale Machines* (third ed.). Springer, Cham, Switzerland.
- [14] Jose M. Camara, Miquel Moreno, Enrique Vallejo, Ramon Bevide, Jose Miguel-Alonso, Carmen Martinez, and Javier Navaridas. 2010. Twisted Torus Topologies for Enhanced Interconnection Networks. *IEEE Transactions on Parallel and Distributed Systems* 21, 12 (Dec. 2010), 1765–1778. <https://doi.org/10.1109/TPDS.2010.30>
- [15] Bill Chang, Rajiv Kurian, Doug Williams, and Eric Quinell. 2022. DOJO: Super-Compute System Scaling for ML Training. In *2022 IEEE Hot Chips 34 Symposium (HCS)*. IEEE, Cupertino, CA, USA, 1–45. <https://doi.org/10.1109/HCS55958.2022.9895625>
- [16] Shuangliang Chen, Saptadeep Pal, and Rakesh Kumar. 2024. Wafer-scale Network Switches. In *2024 ACM/IEEE 51st Annual International Symposium on Computer Architecture (ISCA)*. IEEE, Buenos Aires, Argentina, 215–229. <https://doi.org/10.1109/ISCA59077.2024.00025>
- [17] Zixiang Chen, Yihe Deng, Yue Wu, Quanquan Gu, and Yuanzhi Li. 2022. Towards Understanding the Mixture-of-Experts Layer in Deep Learning. In *Advances in Neural Information Processing Systems*, S. Koyejo, S. Mohamed, A. Agarwal, D. Belgrave, K. Cho, and A. Oh (Eds.), Vol. 35. Curran Associates, Inc., 23049–23062. https://proceedings.neurips.cc/paper_files/paper/2022/file/91edff07232fb1b55a505a9e9f6c0ff3-Paper-Conference.pdf
- [18] M. Cho, U. Finkler, M. Serrano, D. Kung, and H. Hunter. 2019. BlueConnect: Decomposing All-Reduce for Deep Learning on Heterogeneous Network Hierarchy. *IBM Journal of Research and Development* 63, 6 (Nov. 2019), 1:1–1:11. <https://doi.org/10.1147/JRD.2019.2947013>
- [19] Jack Choquette. 2023. NVIDIA Hopper H100 GPU: Scaling Performance. *IEEE Micro* 43, 3 (May 2023), 9–17. <https://doi.org/10.1109/MM.2023.3256796>

- [20] Shu-Rong Chun, Tin-Hao Kuo, Hao-Yi Tsai, Chung-Shi Liu, Chuei-Tang Wang, Jeng-Shien Hsieh, Tsung-Shu Lin, Terry Ku, and Douglas Yu. 2020. InFO₂SoW (System-on-Wafer) for High Performance Computing. In *2020 IEEE 70th Electronic Components and Technology Conference (ECTC)*. IEEE, Orlando, FL, USA, 1–6. <https://doi.org/10.1109/ECTC32862.2020.00013>
- [21] Kari A. Clark, Daniel Cletheroe, Thomas Gerard, Istvan Haller, Krzysztof Jozwik, Kai Shi, Benn Thomsen, Hugh Williams, Georgios Zervas, Hitesh Ballani, Polina Bayvel, Paolo Costa, and Zhixin Liu. 2020. Synchronous Subnanosecond Clock and Data Recovery for Optically Switched Data Centres Using Clock Phase Caching. *Nature Electronics* 3, 7 (June 2020), 426–433. <https://doi.org/10.1038/s41928-020-0423-y>
- [22] Damai Dai, Chengqi Deng, Chenggang Zhao, R. X. Xu, Huazuo Gao, Deli Chen, Jiashi Li, Wangding Zeng, Xingkai Yu, Y. Wu, Zhenda Xie, Y. K. Li, Panpan Huang, Fuli Luo, Chong Ruan, Zhifang Sui, and Wenfeng Liang. 2024. DeepSeekMoE: Towards Ultimate Expert Specialization in Mixture-of-Experts Language Models. (Jan. 2024). <https://doi.org/10.48550/arXiv.2401.06066> arXiv:cs/2401.06066
- [23] William J. Dally and Brian Towles. 2004. *Principles and Practices of Interconnection Networks*. Morgan Kaufmann Publishers, Amsterdam ; San Francisco.
- [24] Davide Tonietto. 2023. Energy Efficiency in Serial Links. (Aug. 2023). <https://old.hoti.org/2023/event/diamond-sponsor-talks/index.html>
- [25] Daniele De Sensi, Salvatore Di Girolamo, Kim H. McMahon, Duncan Roweth, and Torsten Hoefler. 2020. An In-Depth Analysis of the Slingshot Interconnect. In *SC20: International Conference for High Performance Computing, Networking, Storage and Analysis*. IEEE, Atlanta, GA, USA, 1–14. <https://doi.org/10.1109/SC41405.2020.00039>
- [26] Daniele De Sensi, Lorenzo Pichetti, Flavio Vella, Tiziano De Matteis, Zebin Ren, Luigi Fusco, Matteo Turisini, Daniele Cesarini, Kurt Lust, Animesh Trivedi, Duncan Roweth, Filippo Spiga, Salvatore Di Girolamo, and Torsten Hoefler. 2024. Exploring GPU-to-GPU Communication: Insights into Supercomputer Interconnects. In *Proceedings of the International Conference for High Performance Computing, Networking, Storage, and Analysis (Sc '24)*. IEEE Press, Atlanta, GA, USA, Article 33. <https://doi.org/10.1109/SC41406.2024.00039>
- [27] DeepSeek-AI, Daya Guo, Dejian Yang, Haowei Zhang, Junxiao Song, Ruoyu Zhang, Runxin Xu, Qihao Zhu, Shirong Ma, Peiyi Wang, Xiao Bi, Xiaokang Zhang, Xingkai Yu, Yu Wu, Z. F. Wu, Zhibin Gou, Zhihong Shao, Zhuoshu Li, Ziyi Gao, Aixin Liu, Bing Xue, Bingxuan Wang, Bochao Wu, Bei Feng, Chengda Lu, Chenggang Zhao, Chengqi Deng, Chenyu Zhang, Chong Ruan, Damai Dai, Deli Chen, Dongjie Ji, Erhang Li, Fangyun Lin, Fucong Dai, Fuli Luo, Guangbo Hao, Guanting Chen, Guowei Li, H. Zhang, Han Bao, Hanwei Xu, Haocheng Wang, Honghui Ding, Huajian Xin, Huazuo Gao, Hui Qu, Hui Li, Jianzhong Guo, Jiashi Li, Jiawei Wang, Jingchang Chen, Jingyang Yuan, Junjie Qiu, Junlong Li, J. L. Cai, Jiaqi Ni, Jian Liang, Jin Chen, Kai Dong, Kai Hu, Kaige Gao, Kang Guan, Kexin Huang, Kuai Yu, Lean Wang, Lecong Zhang, Liang Zhao, Litong Wang, Liyue Zhang, Lei Xu, Leyi Xia, Mingchuan Zhang, Minghua Zhang, Minghui Tang, Meng Li, Miaojun Wang, Mingming Li, Ning Tian, Panpan Huang, Peng Zhang, Qiancheng Wang, Qinyu Chen, Qiusi Du, Ruiqi Ge, Ruisong Zhang, Ruizhe Pan, Runji Wang, R. J. Chen, R. L. Jin, Ruyi Chen, Shanghao Lu, Shangyan Zhou, Shanhuang Chen, Shengfeng Ye, Shiyu Wang, Shuiping Yu, Shunfeng Zhou, Shuting Pan, S. S. Li, Shuang Zhou, Shaoqing Wu, Shengfeng Ye, Tao Yun, Tian Pei, Tianyu Sun, T. Wang, Wangding Zeng, Wanbiao Zhang, Wen Liu, Wenfeng Liang, Wenjun Gao, Wenqin Yu, Wentao Zhang, W. L. Xiao, Wei An, Xiaodong Liu, Xiaohan Wang, Xiaokang Chen, Xiaotao Nie, Xin Cheng, Xin Liu, Xin Xie, Xingchao Liu, Xinyu Yang, Xinyuan Li, Xuecheng Su, Xuheng Lin, X. Q. Li, Xiangyue Jin, Xiaojin Shen, Xiaosha Chen, Xiaowen Sun, Xiaoxiang Wang, Xinnan Song, Xinyi Zhou, Xianzu Wang, Xinxia Shan, Y. K. Li, Y. Q. Wang, Y. X. Wei, Yang Zhang, Yanhong Xu, Yao Li, Yao Zhao, Yaofeng Sun, Yaohui Wang, Yi Yu, Yichao Zhang, Yifan Shi, Yiliang Xiong, Ying He, Yishi Piao, Yisong Wang, Yixuan Tan, Yiyang Ma, Yiyuan Liu, Yongqiang Guo, Yuan Ou, Yudian Wang, Yue Gong, Yuheng Zou, Yujia He, Yunfan Xiong, Yuxiang Luo, Yuxiang You, Yuxuan Liu, Yuyang Zhou, Y. X. Zhu, Yanhong Xu, Yanping Huang, Yaohui Li, Yi Zheng, Yuchen Zhu, Yunxian Ma, Ying Tang, Yukun Zha, Yuting Yan, Z. Z. Ren, Zehui Ren, Zhangli Sha, Zhe Fu, Zhean Xu, Zhenda Xie, Zhengyan Zhang, Zhewen Hao, Zhicheng Ma, Zhigang Yan, Zhiyu Wu, Zihui Gu, Zijia Zhu, Zijun Liu, Zilin Li, Ziwei Xie, Ziyang Song, Zizheng Pan, Zhen Huang, Zhipeng Xu, Zhongyu Zhang, and Zhen Zhang. 2025. DeepSeek-R1: Incentivizing Reasoning Capability in LLMs via Reinforcement Learning. (Jan. 2025). <https://doi.org/10.48550/arXiv.2501.12948> arXiv:cs/2501.12948
- [28] DeepSeek-AI, Aixin Liu, Bei Feng, Bin Wang, Bingxuan Wang, Bo Liu, Chenggang Zhao, Chengqi Deng, Chong Ruan, Damai Dai, Daya Guo, Dejian Yang, Deli Chen, Dongjie Ji, Erhang Li, Fangyun Lin, Fuli Luo, Guangbo Hao, Guanting Chen, Guowei Li, H. Zhang, Hanwei Xu, Hao Yang, Haowei Zhang, Honghui Ding, Huajian Xin, Huazuo Gao, Hui Li, Hui Qu, J. L. Cai, Jian Liang, Jianzhong Guo, Jiaqi Ni, Jiashi Li, Jin Chen, Jingyuan Yuan, Junjie Qiu, Junxiao Song, Kai Dong, Kaige Gao, Kang Guan, Lean Wang, Lecong Zhang, Lei Xu, Leyi Xia, Liang Zhao, Liyue Zhang, Meng Li, Miaojun Wang, Mingchuan Zhang, Minghua Zhang, Minghui Tang, Mingming Li, Ning Tian, Panpan Huang, Peiyi Wang, Peng Zhang, Qihao Zhu, Qinyu Chen, Qiusi Du, R. J. Chen, R. L. Jin, Ruiqi Ge, Ruizhe Pan, Runxin Xu, Ruyi Chen, S. S. Li, Shanghao Lu, Shangyan Zhou, Shanhuang Chen, Shaoqing Wu, Shengfeng Ye, Shirong Ma, Shiyu Wang, Shuang Zhou, Shuiping Yu, Shunfeng Zhou, Size Zheng, T. Wang, Tian Pei, Tianyu Sun, W. L. Xiao, Wangding Zeng, Wei An, Wen Liu, Wenfeng Liang, Wenjun Gao, Wentao Zhang, X. Q. Li, Xiangyue Jin, Xianzu Wang, Xiao Bi, Xiaodong Liu, Xiaohan Wang, Xiaojin Shen, Xiaokang Chen, Xiaosha Chen, Xiaotao Nie, Xiaowen Sun, Xiaoxiang Wang, Xin Liu, Xin Xie, Xingkai Yu, Xinnan Song, Xinyi Zhou, Xinyu Yang, Xuan Lu, Xuecheng Su, Y. Wu, Y. K. Li, Y. X. Wei, Y. X. Zhu, Yanhong Xu, Yanping Huang, Yao Li, Yao Zhao, Yaofeng Sun, Yaohui Li, Yaohui Wang, Yi Zheng, Yichao Zhang, Yiliang Xiong, Yilong Zhao, Ying He, Ying Tang, Yishi Piao, Yixin Dong, Yixuan Tan, Yiyuan Liu, Yongji Wang, Yongqiang Guo, Yuchen Zhu, Yudian Wang, Yuheng Zou, Yukun Zha, Yunxian Ma, Yuting Yan, Yuxiang You, Yuxuan Liu, Z. Z. Ren, Zehui Ren, Zhangli Sha, Zhe Fu, Zhen Huang, Zhen Zhang, Zhenda Xie, Zhewen Hao, Zhihong Shao, Zhiniu Wen, Zhipeng Xu, Zhongyu Zhang, Zhuoshu Li, Zihan Wang, Zihui Gu, Zilin Li, and Ziwei Xie. 2024. DeepSeek-V2: A Strong, Economical, and Efficient Mixture-of-Experts Language Model. (June 2024). <https://doi.org/10.48550/arXiv.2405.04434> arXiv:cs/2405.04434
- [29] DeepSeek-AI, Aixin Liu, Bei Feng, Bing Xue, Bingxuan Wang, Bochao Wu, Chengda Lu, Chenggang Zhao, Chengqi Deng, Chenyu Zhang, Chong Ruan, Damai Dai, Daya Guo, Dejian Yang, Deli Chen, Dongjie Ji, Erhang Li, Fangyun Lin, Fucong Dai, Fuli Luo, Guangbo Hao, Guanting Chen, Guowei Li, H. Zhang, Han Bao, Hanwei Xu, Haocheng Wang, Haowei Zhang, Honghui Ding, Huajian Xin, Huazuo Gao, Hui Li, Hui Qu, J. L. Cai, Jian Liang, Jianzhong Guo, Jiaqi Ni, Jiashi Li, Jiawei Wang, Jin Chen, Jingchang Chen, Jingyang Yuan, Junjie Qiu, Junlong Li, Junxiao Song, Kai Dong, Kai Hu, Kaige Gao, Kang Guan, Kexin Huang, Kuai Yu, Lean Wang, Lecong Zhang, Lei Xu, Leyi Xia, Liang Zhao, Litong Wang, Liyue Zhang, Meng Li, Miaojun Wang, Mingchuan Zhang, Minghua Zhang, Minghui Tang, Mingming Li, Ning Tian, Panpan Huang, Peiyi Wang, Peng Zhang, Qiancheng Wang, Qihao Zhu, Qinyu Chen, Qiusi Du, R. J. Chen, R. L. Jin, Ruiqi Ge, Ruisong Zhang, Ruizhe Pan, Runji Wang, Runxin Xu, Ruoyu

Zhang, Ruyi Chen, S. S. Li, Shanghao Lu, Shangyan Zhou, Shanhuang Chen, Shaoqing Wu, Shengfeng Ye, Shengfeng Ye, Shirong Ma, Shiyu Wang, Shuang Zhou, Shuiping Yu, Shunfeng Zhou, Shuting Pan, T. Wang, Tao Yun, Tian Pei, Tianyu Sun, W. L. Xiao, Wangding Zeng, Wanjia Zhao, Wei An, Wen Liu, Wenfeng Liang, Wenjun Gao, Wenqin Yu, Wentao Zhang, X. Q. Li, Xiangyue Jin, Xianzu Wang, Xiao Bi, Xiaodong Liu, Xiaohan Wang, Xiaojin Shen, Xiaokang Chen, Xiaokang Zhang, Xiaosha Chen, Xiaotao Nie, Xiaowen Sun, Xiaoxiang Wang, Xin Cheng, Xin Liu, Xin Xie, Xingchao Liu, Xingkai Yu, Xinnan Song, Xinxia Shan, Xinyi Zhou, Xinyu Yang, Xinyuan Li, Xuecheng Su, Xuheg Lin, Y. K. Li, Y. Q. Wang, Y. X. Wei, Y. X. Zhu, Yang Zhang, Yanhong Xu, Yanhong Xu, Yanping Huang, Yao Li, Yao Zhao, Yaofeng Sun, Yaohui Li, Yaohui Wang, Yi Yu, Yi Zheng, Yichao Zhang, Yifan Shi, Yiliang Xiong, Ying He, Ying Tang, Yishi Piao, Yisong Wang, Yixuan Tan, Yiyang Ma, Yiyuan Liu, Yongqiang Guo, Yu Wu, Yuan Ou, Yuchen Zhu, Yuduan Wang, Yue Gong, Yuheng Zou, Yujia He, Yukun Zha, Yunfan Xiong, Yunxian Ma, Yuting Yan, Yuxiang Luo, Yuxiang You, Yuxuan Liu, Yuyang Zhou, Z. F. Wu, Z. Z. Ren, Zehui Ren, Zhangli Sha, Zhe Fu, Zhean Xu, Zhen Huang, Zhen Zhang, Zhenda Xie, Zhengyan Zhang, Zhewen Hao, Zhibin Gou, Zhicheng Ma, Zhigang Yan, Zhihong Shao, Zhipeng Xu, Zhiyu Wu, Zhongyu Zhang, Zhuoshu Li, Zihui Gu, Zijia Zhu, Zijun Liu, Zilin Li, Ziwei Xie, Ziyang Song, Ziyi Gao, and Zizheng Pan. 2024. DeepSeek-V3 Technical Report. (Dec. 2024). <https://doi.org/10.48550/arXiv.2412.19437> arXiv:cs/2412.19437

- [30] Douglas Yu. 2021. TSMC Packaging Technologies for Chiplets and 3D. In *Proceedings of the 2021 IEEE Hot Chips (HCS)*.
- [31] Jiangfei Duan, Shuo Zhang, Zerui Wang, Lijuan Jiang, Wenwen Qu, Qinghao Hu, Guoteng Wang, Qizhen Weng, Hang Yan, Xingcheng Zhang, Xipeng Qiu, Dahua Lin, Yonggang Wen, Xin Jin, Tianwei Zhang, and Peng Sun. 2024. Efficient Training of Large Language Models on Distributed Infrastructures: A Survey. (July 2024). arXiv:cs/2407.20018 <http://arxiv.org/abs/2407.20018>
- [32] Abhimanyu Dubey, Abhinav Jauhri, Abhinav Pandey, Abhishek Kadian, Ahmad Al-Dahle, Aiesha Letman, Akhil Mathur, Alan Schelten, Amy Yang, Angela Fan, Anirudh Goyal, Anthony Hartshorn, Aobo Yang, Archi Mitra, Archie Sravankumar, Artem Korenev, Arthur Hinsvark, Arun Rao, Aston Zhang, Aurelien Rodriguez, Austen Gregerson, Ava Spataru, Baptiste Roziere, Bethany Biron, Binh Tang, Bobbie Chern, Charlotte Caucheteux, Chaya Nayak, Chloe Bi, Chris Marra, Chris McConnell, Christian Keller, Christophe Touret, Chunyang Wu, Corinne Wong, Cristian Canton Ferrer, Cyrus Nikolaidis, Damien Allonsius, Daniel Song, Danielle Pintz, Danny Livshits, David Esobu, Dhruv Choudhary, Dhruv Mahajan, Diego Garcia-Olano, Diego Perino, Dieuwke Hupkes, Egor Lakomkin, Ehab AlBadawy, Elina Lobanova, Emily Dinan, Eric Michael Smith, Filip Radenovic, Frank Zhang, Gabriel Synnaeve, Gabrielle Lee, Georgia Lewis Anderson, Graeme Nail, Gregoire Mialon, Guan Pang, Guillem Cucurell, Hailey Nguyen, Hannah Korevaar, Hu Xu, Hugo Touvron, Iliyan Zarov, Imanol Arrieta Ibarra, Isabel Kloumann, Ishan Misra, Ivan Evtimov, Jade Copet, Jaewon Lee, Jan Geffert, Jana Vranes, Jason Park, Jay Mahadeokar, Jeet Shah, Jelmer van der Linde, Jennifer Billock, Jenny Hong, Jenya Lee, Jeremy Fu, Jianfeng Chi, Jianyu Huang, Jiawen Liu, Jie Wang, Jiecao Yu, Joanna Bitton, Joe Spisak, Jongsoo Park, Joseph Rocca, Joshua Johnstun, Joshua Saxe, Junteng Jia, Kalyan Vasuden Alwala, Kartikeya Upasani, Kate Plawiak, Ke Li, Kenneth Heafield, Kevin Stone, Khalid El-Arini, Krithika Iyer, Kshitiz Malik, Kuenley Chiu, Kunal Bhalla, Lauren Rantala-Young, Laurent van der Maaten, Lawrence Chen, Liang Tan, Liz Jenkins, Louis Martin, Lovish Madaan, Lubo Malo, Lukas Blecher, Lukas Landzaat, Luke de Oliveira, Madeline Muzzi, Mahesh Pasupuleti, Mannat Singh, Manohar Paluri, Marcin Kardas, Mathew Oldham, Mathieu Rita, Maya

Pavlova, Melanie Kambadur, Mike Lewis, Min Si, Mitesh Kumar Singh, Mona Hassan, Naman Goyal, Narjes Torabi, Nikolay Bashlykov, Nikolay Bogoychev, Niladri Chatterji, Olivier Duchenne, Onur Çelebi, Patrick Alrassy, Pengchuan Zhang, Pengwei Li, Petar Vasic, Peter Weng, Prajjwal Bhargava, Pratik Dubal, Praveen Krishnan, Punit Singh Koura, Puxin Xu, Qing He, Qingxiao Dong, Ragavan Srinivasan, Raj Ganapathy, Ramon Calderer, Ricardo Silveira Cabral, Robert Stojnic, Roberta Raileanu, Rohit Girdhar, Rohit Patel, Romain Sauvestre, Ronnie Polidoro, Roshan Sumbaly, Ross Taylor, Ruan Silva, Rui Hou, Rui Wang, Saghar Hosseini, Sahana Chennabasappa, Sanjay Singh, Sean Bell, Seohyun Sonia Kim, Sergey Edunov, Shaoliang Nie, Sharan Narang, Sharath Rapparthi, Sheng Shen, Shengye Wan, Shruti Bhosale, Shun Zhang, Simon Vandenhende, Soumya Batra, Spencer Whitman, Sten Sootla, Stephane Collot, Suchin Gururangan, Sydney Borodinsky, Tamar Herman, Tara Fowler, Tarek Sheasha, Thomas Georgiou, Thomas Scialom, Tobias Speckbacher, Todor Mihaylov, Tong Xiao, Ujjwal Karn, Vedanuj Goswami, Vibhor Gupta, Vignesh Ramanathan, Viktor Kerkez, Vincent Gonguet, Virginie Do, Vish Vogeti, Vladan Petrovic, Weiwei Chu, Wenhan Xiong, Wenyin Fu, Whitney Meers, Xavier Martinet, Xiaodong Wang, Xiaoqing Ellen Tan, Xinfeng Xie, Xuchao Jia, Xuewei Wang, Yaelle Goldschlag, Yashesh Gaur, Yasmine Babaei, Yi Wen, Yiwen Song, Yuchen Zhang, Yue Li, Yuning Mao, Zacharie Delprat, Zhen Yan, Zhengxing Chen, Zoe Papakipos, Aaditya Singh, Aaron Grattafiori, Abha Jain, Adam Kelsey, Adam Shajnfeld, Adithya Gangidi, Adolfo Victoria, Ahuva Goldstand, Ajay Menon, Ajay Sharma, Alex Boesenberg, Alex Vaughan, Alexei Baevski, Allie Feinstein, Amanda Kallet, Amit Sangani, Anam Yunus, Andrei Lupu, Andres Alvarado, Andrew Caples, Andrew Gu, Andrew Ho, Andrew Poulton, Andrew Ryan, Ankit Ramchandani, Annie Franco, Aparajita Saraf, Arkabandhu Chowdhury, Ashley Gabriel, Ashwin Bharambe, Assaf Eisenman, Azadeh Yazdan, Beau James, Ben Maurer, Benjamin Leonhardi, Bernie Huang, Beth Loyd, Beto De Paola, Bhargavi Paranjape, Bing Liu, Bo Wu, Boyu Ni, Braden Hancock, Bram Wasti, Brandon Spence, Brani Stojkovic, Brian Gamido, Britt Montalvo, Carl Parker, Carly Burton, Catalina Mejia, Changhan Wang, Changkyu Kim, Chao Zhou, Chester Hu, Ching-Hsiang Chu, Chris Cai, Chris Tindal, Christoph Feichtenhofer, Damon Civin, Dana Beaty, Daniel Kreymer, Daniel Li, Danny Wyatt, David Adkins, David Xu, Davide Testuggine, Delia David, Devi Parikh, Diana Liskovich, Didem Foss, Dingkang Wang, Duc Le, Dustin Holland, Edward Dowling, Eissa Jamil, Elaine Montgomerie, Eleonora Presani, Emily Hahn, Emily Wood, Erik Brinkman, Esteban Arcaute, Evan Dunbar, Evan Smothers, Fei Sun, Felix Kreuk, Feng Tian, Firat Ozgenel, Francesco Caggioni, Francisco Guzmán, Frank Kanayet, Frank Seide, Gabriela Medina Florez, Gabriella Schwarz, Gada Badeer, Georgia Swee, Gil Halpern, Govind Thattai, Grant Herman, Gregory Sizov, Guangyi, Zhang, Guna Lakshminarayanan, Hamid Shojanazeri, Han Zou, Hannah Wang, Hanwen Zha, Haroun Habeeb, Harrison Rudolph, Helen Suk, Henry Aspegren, Hunter Goldman, Igor Molybog, Igor Tufanov, Irina-Elena Veliche, Itai Gat, Jake Weissman, James Geboski, James Kohli, Japhet Asher, Jean-Baptiste Gaya, Jeff Marcus, Jeff Tang, Jennifer Chan, Jenny Zhen, Jeremy Reizenstein, Jeremy Teboul, Jessica Zhong, Jian Jin, Jingyi Yang, Joe Cummings, Jon Carvill, Jon Shepard, Jonathan McPhee, Jonathan Torres, Josh Ginsburg, Junjie Wang, Kai Wu, Kam Hou U, Karan Saxena, Karthik Prasad, Kartikay Khandelwal, Katayoun Zand, Kathy Matosich, Kaushik Veeraraghavan, Kelly Michelen, Keqian Li, Kun Huang, Kunal Chawla, Kushal Lakhotia, Kyle Huang, Lailin Chen, Lakshya Garg, Lavender A, Leandro Silva, Lee Bell, Lei Zhang, Liangpeng Guo, Licheng Yu, Liron Moshkovich, Luca Wehrstedt, Madian Khabsa, Manav Avalani, Manish Bhatt, Maria Tsimpoukelli, Martynas Mankus, Matan Hasson, Matthew Lennie, Matthias Reso, Maxim Groshev,

- Maxim Naumov, Maya Lathi, Meghan Keneally, Michael L. Seltzer, Michal Valko, Michelle Restrepo, Mihir Patel, Mik Vyatskov, Mikayel Samvelyan, Mike Clark, Mike Macey, Mike Wang, Miquel Jubert Hermoso, Mo Metanat, Mohammad Rastegari, Munish Bansal, Nandhini Santhanam, Natascha Parks, Natasha White, Navyata Bawa, Nayan Singhal, Nick Egebo, Nicolas Usunier, Nikolay Pavlovich Laptev, Ning Dong, Ning Zhang, Norman Cheng, Oleg Chernoguz, Olivia Hart, Omkar Salpekar, Ozlem Kalinli, Parkin Kent, Parth Parekh, Paul Saab, Pavan Balaji, Pedro Rittner, Philip Bontrager, Pierre Roux, Piotr Dollar, Polina Zvyagina, Prashant Ratanchandani, Pritish Yuvraj, Qian Liang, Rachad Alao, Rachel Rodriguez, Rafi Ayub, Raghobham Murthy, Raghu Nayani, Rahul Mitra, Raymond Li, Rebekkah Hogan, Robin Battey, Rocky Wang, Rohan Maheswari, Russ Howes, Ruty Rinott, Sai Jayesh Bondu, Samyak Datta, Sara Chugh, Sara Hunt, Sargun Dhillon, Sasha Sidorov, Satadru Pan, Saurabh Verma, Seiji Yamamoto, Sharadh Ramaswamy, Shaun Lindsay, Shaun Lindsay, Sheng Feng, Shenghao Lin, Shengxin Cindy Zha, Shiva Shankar, Shuqiang Zhang, Shuqiang Zhang, Sinong Wang, Sneha Agarwal, Soji Sajuyigbe, Soumith Chintala, Stephanie Max, Stephen Chen, Steve Kehoe, Steve Satterfield, Sudarshan Govindaprasad, Sumit Gupta, Sungmin Cho, Sunny Virk, Suraj Subramanian, Sy Choudhury, Sydney Goldman, Tal Remez, Tamar Glaser, Tamara Best, Thilo Kohler, Thomas Robinson, Tianhe Li, Tianjun Zhang, Tim Matthews, Timothy Chou, Tzook Shaked, Varun Vontimitta, Victoria Ajayi, Victoria Montanez, Vijai Mohan, Vinay Satish Kumar, Vishal Mangla, Vlad Ionescu, Vlad Poenaru, Vlad Tiberiu Mihailescu, Vladimir Ivanov, Wei Li, Wenchen Wang, Wenwen Jiang, Wes Bouaziz, Will Constable, Xiaocheng Tang, Xiaofang Wang, Xiaojuan Wu, Xiaolan Wang, Xide Xia, Xilun Wu, Xinbo Gao, Yanjun Chen, Ye Hu, Ye Jia, Ye Qi, Yenda Li, Yilin Zhang, Ying Zhang, Yossi Adi, Youngjin Nam, Yu, Wang, Yuchen Hao, Yundi Qian, Yuzi He, Zach Rait, Zachary DeVito, Zef Rosnbrick, Zhaoduo Wen, Zhenyu Yang, and Zhiwei Zhao. 2024. The Llama 3 Herd of Models. (July 2024). arXiv:cs/2407.21783 <http://arxiv.org/abs/2407.21783>
- [33] Anne C. Elster and Tor A. Haugdahl. 2022. Nvidia Hopper GPU and Grace CPU Highlights. *Computing in Science & Engineering* 24, 2 (March 2022), 95–100. <https://doi.org/10.1109/MCSE.2022.3163817>
- [34] Saeed Fatholouloumi. 2024. 4 Tb/s Optical Compute Interconnect Chiplet for XPU-to-XPU Connectivity. In *2024 IEEE Hot Chips 36 Symposium (HCS)*. IEEE, Stanford, CA, USA, 1–18. <https://doi.org/10.1109/HCS61935.2024.10665032>
- [35] William Fedus, Barret Zoph, and Noam Shazeer. 2022. Switch Transformers: Scaling to Trillion Parameter Models with Simple and Efficient Sparsity. (June 2022). <https://doi.org/10.48550/arXiv.2101.03961> arXiv:cs/2101.03961
- [36] Yinxiao Feng and Kaisheng Ma. 2024. Switch-Less Dragonfly on Wafers: A Scalable Interconnection Architecture Based on Wafer-Scale Integration. In *SC24: International Conference for High Performance Computing, Networking, Storage and Analysis*. IEEE, Atlanta, GA, USA, 1–17. <https://doi.org/10.1109/SC41406.2024.00102>
- [37] Yinxiao Feng, Yuchen Wei, Dong Xiang, and Kaisheng Ma. 2024. Evaluating Chiplet-Based Large-Scale Interconnection Networks via Cycle-Accurate Packet-Parallel Simulation. In *2024 USENIX Annual Technical Conference (USENIX ATC 24)*. USENIX Association, Santa Clara, CA, USA, 731–747. <https://www.usenix.org/conference/atc24/presentation/feng-yinxiao>
- [38] Yinxiao Feng, Dong Xiang, and Kaisheng Ma. 2023. A Scalable Methodology for Designing Efficient Interconnection Network of Chiplets. In *2023 IEEE International Symposium on High-Performance Computer Architecture (HPCA)*. IEEE, Montreal, QC, Canada, 1059–1071. <https://doi.org/10.1109/HPCA56546.2023.10070981>
- [39] Michael Y. Frankel. 2021. Prospects for Optical Transceivers Expanding to Access, Metro and Long-Haul. In *Optical Fiber Communication Conference (OFC) 2021*. Optica Publishing Group, Washington, DC, Tu5A.2. <https://doi.org/10.1364/OFC.2021.Tu5A.2>
- [40] Mingye Fu, Guangyao Liu, Roberto Proietti, Yichi Zhang, and S. J. Ben Yoo. 2021. First Demonstration of Monolithic Silicon Photonic Integrated Circuit 32×32 Thin-CLOS AWGR for All-to-All Interconnections. In *2021 European Conference on Optical Communication (ECOC)*. IEEE, Bordeaux, France, 1–4. <https://doi.org/10.1109/ECOC52684.2021.9605973>
- [41] Adithya Gangidi, Rui Miao, Shengbao Zheng, Sai Jayesh Bondu, Guilherme Goes, Hany Morsy, Rohit Puri, Mohammad Riffati, Ashmitha Jeevaraj Shetty, Jingyi Yang, Shuqiang Zhang, Mikel Jimenez Fernandez, Shashidhar Gandham, and Hongyi Zeng. 2024. RDMA over Ethernet for Distributed Training at Meta Scale. In *Proceedings of the ACM SIGCOMM 2024 Conference*. ACM, Sydney NSW Australia, 57–70. <https://doi.org/10.1145/3651890.3672233>
- [42] Alexandru M. Gherghescu, Vlad-Andrei Bădoiu, Alexandru Agache, Mihai-Valentin Dumitru, Iuliu Vasilescu, Radu Mantu, and Costin Raiciu. 2024. I’ve Got 99 Problems But FLOPS Ain’t One. In *Proceedings of the 23rd ACM Workshop on Hot Topics in Networks*. ACM, Irvine CA USA, 195–204. <https://doi.org/10.1145/3696348.3696893>
- [43] Alexandru M. Gherghescu, Vlad-Andrei Bădoiu, Alexandru Agache, Mihai-Valentin Dumitru, Iuliu Vasilescu, Radu Mantu, and Costin Raiciu. 2024. A Look Into Training Large Language Models on Next Generation Datacenters. (July 2024). arXiv:cs/2407.12819 <http://arxiv.org/abs/2407.12819>
- [44] C.J. Glass and L.M. Ni. 1992. The Turn Model for Adaptive Routing. In *Proceedings the 19th Annual International Symposium on Computer Architecture*. IEEE, Gold Coast, Australia, 278–287. <https://doi.org/10.1109/ISCA.1992.753324>
- [45] Google. 2024. TPU v4 Document. <https://cloud.google.com/tpu/docs/v4>. (2024). <https://cloud.google.com/tpu/docs/v4>
- [46] Albert Greenberg, James Hamilton, David A. Maltz, and Parveen Patel. 2008. The Cost of a Cloud: Research Problems in Data Center Networks. *ACM SIGCOMM Computer Communication Review* 39, 1 (Dec. 2008), 68–73. <https://doi.org/10.1145/1496091.1496103>
- [47] Chuanxiong Guo, Guohan Lu, Dan Li, Haitao Wu, Xuan Zhang, Yunfeng Shi, Chen Tian, Yongguang Zhang, and Songwu Lu. 2009. BCube: A High Performance, Server-Centric Network Architecture for Modular Data Centers. In *Proceedings of the ACM SIGCOMM 2009 Conference on Data Communication*. ACM, Barcelona Spain, 63–74. <https://doi.org/10.1145/1592568.1592577>
- [48] Torsten Hoefler, Tommaso Bonato, Daniele De Sensi, Salvatore Di Girolamo, Shigang Li, Marco Heddes, Jon Belk, Deepak Goel, Miguel Castro, and Steve Scott. 2022. HammingMesh: A Network Topology for Large-Scale Deep Learning. In *SC22: International Conference for High Performance Computing, Networking, Storage and Analysis*. IEEE, Dallas, TX, USA, 1–18. <https://doi.org/10.1109/SC41404.2022.00016>
- [49] Jason Howard. 2023. The First Direct Mesh-to-Mesh Photonic Fabric. In *2023 IEEE Hot Chips 35 Symposium (HCS)*. IEEE, Palo Alto, CA, USA, 1–17. <https://doi.org/10.1109/HCS59251.2023.10254719>
- [50] Yang Hu, Xinhan Lin, Huizheng Wang, Zhen He, Xingmao Yu, Jiahao Zhang, Qize Yang, Zheng Xu, Sihan Guan, Jiahao Fang, Hao-ran Shang, Xinru Tang, Xu Dai, Shaojun Wei, and Shouyi Yin. 2024. Wafer-Scale Computing: Advancements, Challenges, and Future Perspectives [Feature]. *IEEE Circuits and Systems Magazine* 24, 1 (2024), 52–81. <https://doi.org/10.1109/MCAS.2024.3349669>
- [51] Yanping Huang, Youlong Cheng, Ankur Bapna, Orhan Firat, Dehao Chen, Mia Chen, HyoukJoong Lee, Jiquan Ngiam, Quoc V Le, Yonghui Wu, and zhifeng Chen. 2019. GPipe: Efficient Training of Giant Neural

- Networks Using Pipeline Parallelism. In *Advances in Neural Information Processing Systems*, H. Wallach, H. Larochelle, A. Beygelzimer, F. dAlché-Buc, E. Fox, and R. Garnett (Eds.), Vol. 32. Curran Associates, Inc. https://proceedings.neurips.cc/paper_files/paper/2019/file/093f65e080a295f8076b1c5722a46aa2-Paper.pdf
- [52] Patrick Iff, Maciej Besta, Matheus Cavalcante, Tim Fischer, Luca Benini, and Torsten Hoefler. 2023. HexaMesh: Scaling to Hundreds of Chiplets with an Optimized Chiplet Arrangement. In *2023 60th ACM/IEEE Design Automation Conference (DAC)*. IEEE, San Francisco, CA, USA, 1–6. <https://doi.org/10.1109/DAC56929.2023.10248006>
- [53] Alexander Ishii and Ryan Wells. 2022. The Nvlink-Network Switch: Nvidia’s Switch Chip for High Communication-Bandwidth Superpods. In *2022 IEEE Hot Chips 34 Symposium (HCS)*. IEEE, Cupertino, CA, USA, 1–23. <https://doi.org/10.1109/HCS55958.2022.9895480>
- [54] Sam Ade Jacobs, Masahiro Tanaka, Chengming Zhang, Minjia Zhang, Shuaiwen Leon Song, Samyam Rajbhandari, and Yuxiong He. 2023. DeepSpeed Llysesse: System Optimizations for Enabling Training of Extreme Long Sequence Transformer Models. (Oct. 2023). [arXiv:cs/2309.14509](https://arxiv.org/abs/2309.14509) <http://arxiv.org/abs/2309.14509>
- [55] Albert Q. Jiang, Alexandre Sablayrolles, Antoine Roux, Arthur Mensch, Blanche Savary, Chris Bamford, Devendra Singh Chaplot, Diego de las Casas, Emma Bou Hanna, Florian Bressand, Gianna Lengyel, Guillaume Bour, Guillaume Lample, Léo Renard Lavaud, Lucile Saulnier, Marie-Anne Lachaux, Pierre Stock, Sandeep Subramanian, Sophia Yang, Szymon Antoniak, Teven Le Scao, Théophile Gervet, Thibaut Lavril, Thomas Wang, Timothée Lacroix, and William El Sayed. 2024. Mixtral of Experts. (Jan. 2024). <https://doi.org/10.48550/arXiv.2401.04088> [arXiv:cs/2401.04088](https://arxiv.org/abs/2401.04088)
- [56] Nan Jiang, James Balfour, Daniel U. Becker, Brian Towles, William J. Dally, George Michelogiannakis, and John Kim. 2013. A Detailed and Flexible Cycle-Accurate Network-on-Chip Simulator. In *2013 IEEE International Symposium on Performance Analysis of Systems and Software (ISPASS)*. IEEE, Austin, TX, USA, 86–96. <https://doi.org/10.1109/ISPASS.2013.6557149>
- [57] Ziheng Jiang, Haibin Lin, Yinmin Zhong, Qi Huang, Yangrui Chen, Zhi Zhang, Yanghua Peng, Xiang Li, Cong Xie, Shibiao Nong, Yulu Jia, Sun He, Hongmin Chen, Zhihao Bai, Qi Hou, Shipeng Yan, Ding Zhou, Yiyao Sheng, Zhuo Jiang, Haohan Xu, Haoran Wei, Zhang Zhang, Pengfei Nie, Leqi Zou, Sida Zhao, Liang Xiang, Zherui Liu, Zhe Li, Xiaoying Jia, Jianxi Ye, Xin Jin, and Xin Liu. 2024. MegaScale: Scaling Large Language Model Training to More Than 10,000 GPUs. In *21st USENIX Symposium on Networked Systems Design and Implementation (NSDI 24)*. USENIX Association, Santa Clara, CA, 745–760. <https://www.usenix.org/conference/nsdi24/presentation/jiang-ziheng>
- [58] Norm Jouppi, George Kurian, Sheng Li, Peter Ma, Rahul Nagarajan, Lifeng Nai, Nishant Patil, Suvinay Subramanian, Andy Swing, Brian Towles, Clifford Young, Xiang Zhou, Zongwei Zhou, and David A Patterson. 2023. TPU v4: An Optically Reconfigurable Supercomputer for Machine Learning with Hardware Support for Embeddings. In *Proceedings of the 50th Annual International Symposium on Computer Architecture*. ACM, Orlando FL USA, 1–14. <https://doi.org/10.1145/3579371.3589350>
- [59] Jared Kaplan, Sam McCandlish, Tom Henighan, Tom B. Brown, Benjamin Chess, Rewon Child, Scott Gray, Alec Radford, Jeffrey Wu, and Dario Amodei. 2020. Scaling Laws for Neural Language Models. (Jan. 2020). [arXiv:cs, stat/2001.08361](https://arxiv.org/abs/2001.08361) <http://arxiv.org/abs/2001.08361>
- [60] M. R. Siavash Katebzadeh, Paolo Costa, and Boris Grot. 2020. Evaluation of an InfiniBand Switch: Choose Latency or Bandwidth, but Not Both. In *2020 IEEE International Symposium on Performance Analysis of Systems and Software (ISPASS)*. IEEE, Boston, MA, USA, 180–191. <https://doi.org/10.1109/ISPASS48437.2020.00033>
- [61] Kevin Zhang. 2024. An Option Besides CoWoS: System-on-Wafer (TSMC-SoW). (2024).
- [62] Mehrdad Khani, Manya Ghobadi, Mohammad Alizadeh, Ziyi Zhu, Madeleine Glick, Keren Bergman, Amin Vahdat, Benjamin Klenk, and Eiman Ebrahimi. 2021. SiP-ML: High-Bandwidth Optical Network Interconnects for Machine Learning Training. In *Proceedings of the 2021 ACM SIGCOMM 2021 Conference*. ACM, Virtual Event USA, 657–675. <https://doi.org/10.1145/3452296.3472900>
- [63] John Kim, William J. Dally, Steve Scott, and Dennis Abts. 2008. Technology-Driven, Highly-Scalable Dragonfly Topology. In *2008 International Symposium on Computer Architecture*. IEEE, Beijing, China, 77–88. <https://doi.org/10.1109/ISCA.2008.19>
- [64] Vijay Korthikanti, Jared Casper, Sangkug Lym, Lawrence McAfee, Michael Andersch, Mohammad Shoeybi, and Bryan Catanzaro. 2022. Reducing Activation Recomputation in Large Transformer Models. (May 2022). [arXiv:cs/2205.05198](https://arxiv.org/abs/2205.05198) <http://arxiv.org/abs/2205.05198>
- [65] Tushar Krishna. 2017. Garnet2.0: A Detailed On-Chip Network Model Inside a Full-System Simulator. (2017).
- [66] Sameer Kumar and Norm Jouppi. 2020. Highly Available Data Parallel ML Training on Mesh Networks. (Nov. 2020). [arXiv:cs/2011.03605](https://arxiv.org/abs/2011.03605) <http://arxiv.org/abs/2011.03605>
- [67] Sabuj Laskar, Pranati Majhi, Sungkeun Kim, Farabi Mahmud, Abdullah Muzahid, and Eun Jung Kim. 2024. Enhancing Collective Communication in MCM Accelerators for Deep Learning Training. In *2024 IEEE International Symposium on High-Performance Computer Architecture (HPCA)*. IEEE, Edinburgh, United Kingdom, 1–16. <https://doi.org/10.1109/HPCA57654.2024.00069>
- [68] John H. Lau. 2019. Recent Advances and Trends in Fan-Out Wafer/Panel-Level Packaging. *Journal of Electronic Packaging* 141, 4 (Dec. 2019), 040801. <https://doi.org/10.1115/1.4043341>
- [69] Dmitry Lepikhin, HyoukJoong Lee, Yuanzhong Xu, Dehao Chen, Orhan Firat, Yanping Huang, Maxim Krikun, Noam Shazeer, and Zhifeng Chen. 2020. GShard: Scaling Giant Models with Conditional Computation and Automatic Sharding. (June 2020). [arXiv:cs, stat/2006.16668](https://arxiv.org/abs/2006.16668) <http://arxiv.org/abs/2006.16668>
- [70] Hong Liu, Ryohei Urata, Kevin Yasumura, Xiang Zhou, Roy Bannon, Jill Berger, Pedram Dashti, Norm Jouppi, Cedric Lam, Sheng Li, Erji Mao, Daniel Nelson, George Papen, Mukarram Tariq, and Amin Vahdat. 2023. Lightwave Fabrics: At-Scale Optical Circuit Switching for Datacenter and Machine Learning Systems. In *Proceedings of the ACM SIGCOMM 2023 Conference*. ACM, New York NY USA, 499–515. <https://doi.org/10.1145/3603269.3604836>
- [71] Hao Liu, Matej Zaharia, and Pieter Abbeel. 2023. Ring Attention with Blockwise Transformers for Near-Infinite Context. (Nov. 2023). [arXiv:cs/2310.01889](https://arxiv.org/abs/2310.01889) <http://arxiv.org/abs/2310.01889>
- [72] Kefei Liu, Jiao Zhang, Zhuo Jiang, Xuan Zhang, Shixian Guo, Yangyang Bai, Yongbin Dong, Zhang Zhang, Xiang Shi, Lei Wang, Haoran Wei, Zicheng Wang, Yongchen Pan, Tian Pan, and Tao Huang. 2024. Hostmesh: Monitor and Diagnose Networks in Rail-Optimized RoCE Clusters. In *Proceedings of the 8th Asia-Pacific Workshop on Networking*. ACM, Sydney Australia, 122–128. <https://doi.org/10.1145/3663408.3663426>
- [73] Xuting Liu, Behnaz Arzani, Siva Kesava Reddy Kakarla, Liangyu Zhao, Vincent Liu, Miguel Castro, Srikanth Kandula, and Luke Marshall. 2024. Rethinking Machine Learning Collective Communication as a Multi-Commodity Flow Problem. In *Proceedings of the ACM SIGCOMM 2024 Conference*. ACM, Sydney NSW Australia, 16–37. <https://doi.org/10.1145/3651890.3672249>
- [74] Lizhong Chen and T. M. Pinkston. 2013. Worm-Bubble Flow Control. In *2013 IEEE 19th International Symposium on High Performance Computer Architecture (HPCA)*. IEEE, Shenzhen, 366–377. <https://doi.org/10.1109/HPCA.2013.6522333>

- [75] Piotr Luczynski, Lukas Gianinazzi, Patrick Iff, Leighton Wilson, Daniele De Sensi, and Torsten Hoefler. 2024. Near-Optimal Wafer-Scale Reduce. In *Proceedings of the 33rd International Symposium on High-Performance Parallel and Distributed Computing*. ACM, Pisa Italy, 334–347. <https://doi.org/10.1145/3625549.3658693>
- [76] Pavlos Maniotis and Daniel M. Kuchta. 2024. Exploring the Benefits of Using Co-Packaged Optics in Data Center and AI Supercomputer Networks: A Simulation-Based Analysis [Invited]. *Journal of Optical Communications and Networking* 16, 2 (Feb. 2024), A143. <https://doi.org/10.1364/JOCN.501427>
- [77] Nie McDonald, Mikhail Isaev, Adriana Flores, Al Davis, and John Kim. 2019. Practical and Efficient Incremental Adaptive Routing for HyperX Networks. In *Proceedings of the International Conference for High Performance Computing, Networking, Storage and Analysis*. ACM, Denver Colorado, 1–13. <https://doi.org/10.1145/3295500.3356151>
- [78] Manish Mehta. 2024. An AI Compute ASIC with Optical Attach to Enable Next Generation Scale-Up Architectures. In *2024 IEEE Hot Chips 36 Symposium (HCS)*. IEEE, Stanford, CA, USA, 1–30. <https://doi.org/10.1109/HCS61935.2024.10664787>
- [79] William M. Mellette, Alex Forencich, Rukshani Athapathu, Alex C. Snoeren, George Papen, and George Porter. 2024. Realizing RotorNet: Toward Practical Microsecond Scale Optical Networking. In *Proceedings of the ACM SIGCOMM 2024 Conference*. ACM, Sydney NSW Australia, 392–414. <https://doi.org/10.1145/3651890.3672273>
- [80] Cyriel Minkenberg, Rajagopal Krishnaswamy, Aaron Zilkie, and David Nelson. 2021. Co-packaged Datacenter Optics: Opportunities and Challenges. *IET Optoelectronics* 15, 2 (April 2021), 77–91. <https://doi.org/10.1049/ote2.12020>
- [81] NADDOD. 2024. 64-Port Ethernet Switch,800Gb Managed Switch,L3 4U Switch - NADDOD. <https://www.naddod.com/products/102322.html>. (2024). <https://www.naddod.com/products/102322.html>
- [82] Deepak Narayanan, Mohammad Shoeybi, Jared Casper, Patrick LeGresley, Mostofa Patwary, Vijay Korthikanti, Dmitri Vainbrand, Prethvi Kashinkunti, Julie Bernauer, Bryan Catanzaro, Amar Phanishayee, and Matei Zaharia. 2021. Efficient Large-Scale Language Model Training on GPU Clusters Using Megatron-LM. In *Proceedings of the International Conference for High Performance Computing, Networking, Storage and Analysis*. ACM, St. Louis Missouri, 1–15. <https://doi.org/10.1145/3458817.3476209>
- [83] Maxim Naumov, Dheevatsa Mudigere, Hao-Jun Michael Shi, Jianyu Huang, Narayanan Sundaraman, Jongsoo Park, Xiaodong Wang, Udit Gupta, Carole-Jean Wu, Alisson G. Azzolini, Dmytro Dzhulgakov, Andrey Mallevich, Ilia Cherniavskii, Yinghai Lu, Raghuraman Krishnamoorthi, Ansha Yu, Volodymyr Kondratenko, Stephanie Pereira, Xianjie Chen, Wenlin Chen, Vijay Rao, Bill Jia, Liang Xiong, and Misha Smelyanskiy. 2019. Deep Learning Recommendation Model for Personalization and Recommendation Systems. (May 2019). arXiv:cs/1906.00091 <http://arxiv.org/abs/1906.00091>
- [84] NVIDIA. 2022. Doubling All2all Performance with NVIDIA Collective Communication Library 2.12. <https://developer.nvidia.com/blog/doubling-all2all-performance-with-nvidia-collective-communication-library-2-12/>. (Feb. 2022). <https://developer.nvidia.com/blog/doubling-all2all-performance-with-nvidia-collective-communication-library-2-12/>
- [85] NVIDIA. 2023. NVIDIA DGX SuperPOD: Next Generation Scalable Infrastructure for AI Leadership. <https://docs.nvidia.com/https://docs.nvidia.com/dgx-superpod-reference-architecture-dgx-h100.pdf>. (2023). <https://docs.nvidia.com/https://docs.nvidia.com/dgx-superpod-reference-architecture-dgx-h100.pdf>
- [86] NVIDIA. 2024. Context Parallelism Overview. https://docs.nvidia.com/megatron-core/developer-guide/latest/api-guide/context_parallel.html. (2024). https://docs.nvidia.com/megatron-core/developer-guide/latest/api-guide/context_parallel.html
- [87] NVIDIA. 2024. NVIDIA Grace Hopper Superchip Architecture Whitepaper. <https://resources.nvidia.com/en-us-grace-cpu/nvidia-grace-hopper>. (2024). <https://resources.nvidia.com/en-us-grace-cpu/nvidia-grace-hopper>
- [88] NVIDIA. 2024. NVIDIA Nsight Systems. <https://developer.nvidia.com/nsight-systems>. (2024). <https://developer.nvidia.com/nsight-systems>
- [89] OpenAI, Josh Achiam, Steven Adler, Sandhini Agarwal, Lama Ahmad, Ilge Akkaya, Florencia Leoni Aleman, Diogo Almeida, Janko Altmenschmidt, Sam Altman, Shyamal Anadkat, Red Avila, Igor Babuschkin, Suchir Balaji, Valerie Balcom, Paul Baltescu, Haiming Bao, Mohammad Bavarian, Jeff Belgum, Irwan Bello, Jake Berdine, Gabriel Bernadett-Shapiro, Christopher Berner, Lenny Bogdonoff, Oleg Boiko, Madelaine Boyd, Anna-Luisa Brakman, Greg Brockman, Tim Brooks, Miles Brundage, Kevin Button, Trevor Cai, Rosie Campbell, Andrew Cann, Brittany Carey, Chelsea Carlson, Rory Carmichael, Brooke Chan, Che Chang, Fotis Chantzis, Derek Chen, Sully Chen, Ruby Chen, Jason Chen, Mark Chen, Ben Chess, Chester Cho, Casey Chu, Hyung Won Chung, Dave Cummings, Jeremiah Currier, Yunxing Dai, Cory Decareaux, Thomas Degry, Noah Deutsch, Damien Deville, Arka Dhar, David Dohan, Steve Dowling, Sheila Dunning, Adrien Ecoffet, Atty Eleti, Tyna Eloundou, David Farhi, Liam Fedus, Niko Felix, Simón Posada Fishman, Juston Forte, Isabella Fulford, Leo Gao, Elie Georges, Christian Gibson, Vik Goel, Tarun Gogineni, Gabriel Goh, Rapha Gontijo-Lopes, Jonathan Gordon, Morgan Grafstein, Scott Gray, Ryan Greene, Joshua Gross, Shixiang Shane Gu, Yufei Guo, Chris Hallacy, Jesse Han, Jeff Harris, Yuchen He, Mike Heaton, Johannes Heidecke, Chris Hesse, Alan Hickey, Wade Hickey, Peter Hoeschele, Brandon Houghton, Kenny Hsu, Shengli Hu, Xin Hu, Joost Huizinga, Shantanu Jain, Shawn Jain, Joanne Jang, Angela Jiang, Roger Jiang, Haozhun Jin, Denny Jin, Shino Jomoto, Billie Jonn, Heewoo Jun, Tomer Kaftan, Łukasz Kaiser, Ali Kamali, Ingmar Kanitscheider, Nitish Shirish Keskar, Tabarak Khan, Logan Kilpatrick, Jong Wook Kim, Christina Kim, Yongjik Kim, Jan Hendrik Kirchner, Jamie Kiros, Matt Knight, Daniel Kokotajlo, Łukasz Kondraciuk, Andrew Kondrich, Aris Konstantinidis, Kyle Kosic, Gretchen Krueger, Vishal Kuo, Michael Lampe, Ikai Lan, Teddy Lee, Jan Leike, Jade Leung, Daniel Levy, Chak Ming Li, Rachel Lim, Molly Lin, Stephanie Lin, Mateusz Litwin, Theresa Lopez, Ryan Lowe, Patricia Lue, Anna Makanju, Kim Malfacini, Sam Manning, Todor Markov, Yaniv Markovski, Bianca Martin, Katie Mayer, Andrew Mayne, Bob McGrew, Scott Mayer McKinney, Christine McLeavey, Paul McMillan, Jake McNeil, David Medina, Aalok Mehta, Jacob Menick, Luke Metz, Andrey Mishchenko, Pamela Mishkin, Vinnie Monaco, Evan Morikawa, Daniel Mossing, Tong Mu, Mira Murati, Oleg Murk, David Mély, Ashvin Nair, Reiichiro Nakano, Rajeev Nayak, Arvind Neelakantan, Richard Ngo, Hyeonwoo Noh, Long Ouyang, Cullen O’Keefe, Jakub Pachocki, Alex Paino, Joe Palermo, Ashley Pantuliano, Giambattista Parascandolo, Joel Parish, Emy Parparita, Alex Passos, Mikhail Pavlov, Andrew Peng, Adam Perelman, Filipe de Avila Belbute Peres, Michael Petrov, Henrique Ponde de Oliveira Pinto, Michael, Pokorny, Michelle Pokrass, Vitchyr H. Pong, Tolly Powell, Alethea Power, Boris Power, Elizabeth Proehl, Raul Puri, Alec Radford, Jack Rae, Aditya Ramesh, Cameron Raymond, Francis Real, Kendra Rimbach, Carl Ross, Bob Rotsted, Henri Roussez, Nick Ryder, Mario Saltarelli, Ted Sanders, Shibani Santurkar, Girish Sastry, Heather Schmidt, David Schnurr, John Schulman, Daniel Selsam, Kyla Sheppard, Toki Sherbakov, Jessica Shieh, Sarah Shoker, Pranav Shyam, Szymon Sidor, Eric Sigler, Maddie Simens, Jordan Sitkin, Katarina Slama, Ian Sohl, Benjamin Sokolowsky, Yang Song, Natalie Staudacher, Felipe Petroski Such, Natalie Summers, Ilya Sutskever, Jie Tang, Nikolas Tezak, Madeleine B.

- Thompson, Phil Tillet, Amin Tootoonchian, Elizabeth Tseng, Preston Tuggle, Nick Turley, Jerry Tworek, Juan Felipe Cerón Uribe, Andrea Vallone, Arun Vijayvergiya, Chelsea Voss, Carroll Wainwright, Justin Jay Wang, Alvin Wang, Ben Wang, Jonathan Ward, Jason Wei, C. J. Weinmann, Akila Welihinda, Peter Welinder, Jiayi Weng, Lilian Weng, Matt Wiethoff, Dave Willner, Clemens Winter, Samuel Wolrich, Hannah Wong, Lauren Workman, Sherwin Wu, Jeff Wu, Michael Wu, Kai Xiao, Tao Xu, Sarah Yoo, Kevin Yu, Qiming Yuan, Wojciech Zaremba, Rowan Zellers, Chong Zhang, Marvin Zhang, Shengjia Zhao, Tianhao Zheng, Juntang Zhuang, William Zhuk, and Barret Zoph. 2024. GPT-4 Technical Report. (March 2024). arXiv:cs/2303.08774 <http://arxiv.org/abs/2303.08774>
- [90] Saptadeep Pal, Jingyang Liu, Irina Alam, Nicholas Cebry, Haris Suhail, Shi Bu, Subramanian S. Iyer, Sudhakar Pamarti, Rakesh Kumar, and Puneet Gupta. 2021. Designing a 2048-Chiplet, 14336-Core Waferscale Processor. In *2021 58th ACM/IEEE Design Automation Conference (DAC)*. IEEE, San Francisco, CA, USA, 1183–1188. <https://doi.org/10.1109/DAC18074.2021.9586194>
- [91] Giannis Patronas, Nikos Terzenidis, Prethvi Kashinkunti, Eitan Zahavi, Dimitris Syrivelis, Louis Capps, Zsolt-Alon Wertheimer, Nikos Argyris, Athanasios Fevgas, Craig Thompson, Avraham Ganor, Julie Bernauer, Elad Mentovich, and Paraskevas Bakopoulos. 2025. Optical Switching for Data Centers and Advanced Computing Systems [Invited]. *Journal of Optical Communications and Networking* 17, 1 (Jan. 2025), A87. <https://doi.org/10.1364/JOCN.534317>
- [92] Olusogo Popoola and Bernardi Pranggono. 2018. On Energy Consumption of Switch-Centric Data Center Networks. *The Journal of Supercomputing* 74, 1 (Jan. 2018), 334–369. <https://doi.org/10.1007/s11227-017-2132-5>
- [93] Leon Poutievski, Omid Mashayekhi, Joon Ong, Arjun Singh, Mukarram Tariq, Rui Wang, Jianan Zhang, Virginia Beauregard, Patrick Conner, Steve Gribble, Rishi Kapoor, Stephen Kratzer, Nanfang Li, Hong Liu, Karthik Nagaraj, Jason Ornstein, Samir Sawhney, Ryohei Urata, Lorenzo Vicisano, Kevin Yasumura, Shidong Zhang, Junlan Zhou, and Amin Vahtdat. 2022. Jupiter Evolving: Transforming Google’s Datacenter Network via Optical Circuit Switches and Software-Defined Networking. In *Proceedings of the ACM SIGCOMM 2022 Conference*. ACM, Amsterdam Netherlands, 66–85. <https://doi.org/10.1145/3544216.3544265>
- [94] V. Puente, C. Izu, R. Beivide, J.A. Gregorio, F. Vallejo, and J.M. Prellezo. 2001. The Adaptive Bubble Router. *J. Parallel and Distrib. Comput.* 61, 9 (Sept. 2001), 1180–1208. <https://doi.org/10.1006/jpdc.2001.1746>
- [95] Kun Qian, Yongqing Xi, Jiamin Cao, Jiaqi Gao, Yichi Xu, Yu Guan, Binzhang Fu, Xuemei Shi, Fangbo Zhu, Rui Miao, Chao Wang, Peng Wang, Pengcheng Zhang, Xianlong Zeng, Eddie Ruan, Zhiping Yao, Ennan Zhai, and Dennis Cai. 2024. Alibaba HPN: A Data Center Network for Large Language Model Training. In *Proceedings of the ACM SIGCOMM 2024 Conference*. ACM, Sydney NSW Australia, 691–706. <https://doi.org/10.1145/3651890.3672265>
- [96] Sudarsanan Rajasekaran, Manya Ghobadi, and Aditya Akella. 2024. CASSINI: Network-Aware Job Scheduling in Machine Learning Clusters. In *21st USENIX Symposium on Networked Systems Design and Implementation (NSDI 24)*. 1403–1420. <https://www.usenix.org/conference/nsdi24/presentation/rajasekaran>
- [97] Samyam Rajbhandari, Conglong Li, Zhewei Yao, Minjia Zhang, Reza Yazdani Aminabadi, Ammar Ahmad Awan, Jeff Rasley, and Yuxiong He. 2022. DeepSpeed-MoE: Advancing Mixture-of-Experts Inference and Training to Power next-Generation AI Scale. In *Proceedings of the 39th International Conference on Machine Learning (Proceedings of Machine Learning Research)*, Kamalika Chaudhuri, Stefanie Jegelka, Le Song, Csaba Szepesvari, Gang Niu, and Sivan Sabato (Eds.), Vol. 162. PMLR, 18332–18346. <https://proceedings.mlr.press/v162/rajbhandari22a.html>
- [98] Saeed Rashidi, William Won, Sudarshan Srinivasan, Srinivas Sridharan, and Tushar Krishna. 2022. Themis: A Network Bandwidth-Aware Collective Scheduling Policy for Distributed Training of DL Models. In *Proceedings of the 49th Annual International Symposium on Computer Architecture*. ACM, New York New York, 581–596. <https://doi.org/10.1145/3470496.3527382>
- [99] Carlos Riquelme, Joan Puigcerver, Basil Mustafa, Maxim Neumann, Rodolphe Jenatton, André Susano Pinto, Daniel Keysers, and Neil Houlsby. 2021. Scaling Vision with Sparse Mixture of Experts. (June 2021). arXiv:cs, stat/2106.05974 <http://arxiv.org/abs/2106.05974>
- [100] Omer S. Sella, Andrew W. Moore, and Noa Zilberman. 2018. FEC Killed The Cut-Through Switch. In *Proceedings of the 2018 Workshop on Networking for Emerging Applications and Technologies*. ACM, Budapest Hungary, 15–20. <https://doi.org/10.1145/3229574.3229577>
- [101] Daniele De Sensi, Tommaso Bonato, David Saam, and Torsten Hoefler. 2024. Swing: Short-Cutting Rings for Higher Bandwidth Allreduce. In *21st USENIX Symposium on Networked Systems Design and Implementation (NSDI 24)*. 1445–1462. <https://www.usenix.org/conference/nsdi24/presentation/de-sensi>
- [102] Aashaka Shah, Vijay Chidambaram, Meghan Cowan, Saeed Maleki, Madan Musuvathi, Todd Mytkowicz, Jacob Nelson, Olli Saarikivi, and Rachee Singh. 2023. TACCL: Guiding Collective Algorithm Synthesis Using Communication Sketches. In *20th USENIX Symposium on Networked Systems Design and Implementation (NSDI 23)*. 593–612. <https://www.usenix.org/conference/nsdi23/presentation/shah>
- [103] Noam Shazeer. 2020. GLU Variants Improve Transformer. (Feb. 2020). <https://doi.org/10.48550/arXiv.2002.05202> arXiv:cs/2002.05202
- [104] Noam Shazeer, Azalia Mirhoseini, Krzysztof Maziarz, Andy Davis, Quoc Le, Geoffrey Hinton, and Jeff Dean. 2017. Outrageously Large Neural Networks: The Sparsely-Gated Mixture-of-Experts Layer. (Jan. 2017). <https://doi.org/10.48550/arXiv.1701.06538> arXiv:cs/1701.06538
- [105] Mohammad Shoeybi, Mostofa Patwary, Raul Puri, Patrick LeGresley, Jared Casper, and Bryan Catanzaro. 2020. Megatron-LM: Training Multi-Billion Parameter Language Models Using Model Parallelism. (March 2020). arXiv:cs/1909.08053 <http://arxiv.org/abs/1909.08053>
- [106] Priyank Shukla. 2022. Short Reach Interconnect for the Emerging Multi-Die System Era. (2022). <https://www.ieeetoronto.ca/wp-content/uploads/2022/12/Short-Reach-Interconnect-for-the-Emerging-Multi-Die-System-Era.pdf>
- [107] Siddharth Singh, Olatunji Ruwase, Ammar Ahmad Awan, Samyam Rajbhandari, Yuxiong He, and Abhinav Bhatle. 2023. A Hybrid Tensor-Expert-Data Parallelism Approach to Optimize Mixture-of-Experts Training. In *Proceedings of the 37th International Conference on Supercomputing*. ACM, Orlando FL USA, 203–214. <https://doi.org/10.1145/3577193.3593704>
- [108] Synopsys. 2024. UALink IP Solution | Synopsys. <https://www.synopsys.com/designware-ip/interface-ip/ualink.html>. (2024). <https://www.synopsys.com/designware-ip/interface-ip/ualink.html>
- [109] Emil Talpes, Debjit Das Sarma, Doug Williams, Sahil Arora, Thomas Kunjan, Benjamin Floering, Ankit Jalote, Christopher Hsiong, Chandrasekhar Poorna, Vaidehi Samant, John Sicilia, Anantha Kumar Nivarti, Raghuvir Ramachandran, Tim Fischer, Ben Herzberg, Bill McGee, Ganesh Venkataramanan, and Pete Banon. 2023. The Microarchitecture of DOJO, Tesla’s Exa-Scale Computer. *IEEE Micro* 43, 3 (May 2023), 31–39. <https://doi.org/10.1109/MM.2023.3258906>
- [110] Timothy W Tillson. 1980. A Hamiltonian Decomposition of K_{2m}^* , $2m \geq 8$. *Journal of Combinatorial Theory, Series B* 29, 1 (Aug. 1980), 68–74. [https://doi.org/10.1016/0095-8956\(80\)90044-1](https://doi.org/10.1016/0095-8956(80)90044-1)
- [111] Ajay Tirumala and Raymond Wong. 2024. NVIDIA Blackwell Platform: Advancing Generative AI and Accelerated Computing. In *2024*

- IEEE Hot Chips 36 Symposium (HCS)*. IEEE, Stanford, CA, USA, 1–33. <https://doi.org/10.1109/HCS61935.2024.10665247>
- [112] Davide ToniETTO. 2022. The Future of Short Reach Interconnect. In *ESSCIRC 2022- IEEE 48th European Solid State Circuits Conference (ESSCIRC)*. IEEE, Milan, Italy, 1–8. <https://doi.org/10.1109/ESSCIRC55480.2022.9911398>
- [113] Ryohei Urata, Hong Liu, Kevin Yasumura, Erji Mao, Jill Berger, Xiang Zhou, Cedric Lam, Roy Bannon, Darren Hutchinson, Daniel Nelson, Leon Poutievski, Arjun Singh, Joon Ong, and Amin Vahdat. 2022. Mission Apollo: Landing Optical Circuit Switching at Datacenter Scale. (Aug. 2022). arXiv:cs/2208.10041 <http://arxiv.org/abs/2208.10041>
- [114] Victor Avelar, Patrick Donovan, Paul Lin, Wendy Torell, and Maria A. Torres Arango. 2023. *The AI Disruption: Challenges and Guidance for Data Center Design*. Technical Report. Energy Management Research Center. <https://globalitresearch.com/wp-content/uploads/2024/10/68834-Schneider%20Electric%20CA%20Secure%20Power%20Campaign%20Q3-Q424%20ABM%20Campaign/The%20AI%20Disruption%20Challenges%20and%20Guidance%20for%20Data%20Center%20Design.pdf>
- [115] Songtao Wang, Dan Li, Yang Cheng, Jinkun Geng, Yanshu Wang, Shuai Wang, Shutao Xia, and Jianping Wu. 2020. A Scalable, High-Performance, and Fault-Tolerant Network Architecture for Distributed Machine Learning. *IEEE/ACM Transactions on Networking* 28, 4 (Aug. 2020), 1752–1764. <https://doi.org/10.1109/TNET.2020.2999377>
- [116] Weiyang Wang, Manya Ghobadi, Kayvon Shakeri, Ying Zhang, and Naader Hasani. 2024. Rail-Only: A Low-Cost High-Performance Network for Training LLMs with Trillion Parameters. (July 2024). arXiv:cs/2307.12169 <http://arxiv.org/abs/2307.12169>
- [117] Weiyang Wang, Moein Khazraee, Zhizhen Zhong, Manya Ghobadi, Zhihao Jia, Dheevatsa Mudigere, Ying Zhang, and Anthony Kewitsch. 2023. TopoOpt: Co-Optimizing Network Topology and Parallelization Strategy for Distributed Training Jobs. In *20th USENIX Symposium on Networked Systems Design and Implementation (NSDI 23)*. 739–767. <https://www.usenix.org/conference/nsdi23/presentation/wang-weiyang>
- [118] Weihao Wang, Jie Li, Chuanzhi Wang, Rong Cao, Shunbin Li, Zhiquan Wan, Guandong Liu, Qingwen Deng, and Ruyun Zhang. 2023. Demonstration of a Wafer-Level Integration for System-on-Wafer Architecture. In *2023 24th International Conference on Electronic Packaging Technology (ICEPT)*. IEEE, Shihezi City, China, 1–4. <https://doi.org/10.1109/ICEPT59018.2023.10492385>
- [119] Ying Wei, Yi Chieh Huang, Haiming Tang, Nithya Sankaran, Ish Chadha, Dai Dai, Olakanmi Oluwole, Vishnu Balan, and Edward Lee. 2023. 9.3 NVLink-C2C: A Coherent Off Package Chip-to-Chip Interconnect with 40Gbps/Pin Single-Ended Signaling. In *2023 IEEE International Solid-State Circuits Conference (ISSCC)*. IEEE, San Francisco, CA, USA, 160–162. <https://doi.org/10.1109/ISSCC42615.2023.10067395>
- [120] William Won, Midhilesh Elavazhagan, Sudarshan Srinivasan, Swati Gupta, and Tushar Krishna. 2024. TACOS: Topology-Aware Collective Algorithm Synthesizer for Distributed Machine Learning. In *2024 57th IEEE/ACM International Symposium on Microarchitecture (MICRO)*. IEEE, Austin, TX, USA, 856–870. <https://doi.org/10.1109/MICRO61859.2024.00068>
- [121] Yongji Wu, Yechen Xu, Jingrong Chen, Zhaodong Wang, Ying Zhang, Matthew Lentz, and Danyang Zhuo. 2024. MCCS: A Service-Based Approach to Collective Communication for Multi-Tenant Cloud. In *Proceedings of the ACM SIGCOMM 2024 Conference*. ACM, Sydney NSW Australia, 679–690. <https://doi.org/10.1145/3651890.3672252>
- [122] Charlotte Trueman Have your say. 2024. Nvidia Increases Blackwell Orders from TSMC by 25 Percent; \$1.8m GB200 NVL36 Server Cabinet Expected to Account for Bulk of Deliveries. <https://www.datacenterdynamics.com/en/news/nvidia-increases-blackwell-orders-from-tsmc-by-25-percent-18m-gb200-nvl36-server-cabinet-expected-to-account-for-bulk-of-deliveries/>. (July 2024). <https://www.datacenterdynamics.com/en/news/nvidia-increases-blackwell-orders-from-tsmc-by-25-percent-18m-gb200-nvl36-server-cabinet-expected-to-account-for-bulk-of-deliveries/>
- [123] Dianhai Yu, Liang Shen, Hongxiang Hao, Weibao Gong, Huachao Wu, Jiang Bian, Lirong Dai, and Haoyi Xiong. 2024. MoESys: A Distributed and Efficient Mixture-of-Experts Training and Inference System for Internet Services. (Aug. 2024). arXiv:cs/2205.10034 <http://arxiv.org/abs/2205.10034>
- [124] Tong Zhu, Xiaoye Qu, Daize Dong, Jiacheng Ruan, Jingqi Tong, Conghui He, and Yu Cheng. 2024. LLaMA-MoE: Building Mixture-of-Experts from LLaMA with Continual Pre-Training. (June 2024). arXiv:cs/2406.16554 <http://arxiv.org/abs/2406.16554>
- [125] Yazhou Zu, Alireza Ghaffarkhah, Hoang-Vu Dang, Brian Towles, Steven Hand, Safeen Huda, Adekunle Bello, Alexander Kolbasov, Arash Rezaei, Dayou Du, Steve Lacy, Hang Wang, Aaron Wisner, Chris Lewis, and Henri Bahini. 2024. Resiliency at Scale: Managing Google’s TPUv4 Machine Learning Supercomputer. In *21st USENIX Symposium on Networked Systems Design and Implementation (NSDI 24)*. USENIX Association, Santa Clara, CA, 761–774. <https://www.usenix.org/conference/nsdi24/presentation/zu>

A APPENDICES

A.1 Hamiltonian Decomposition of Complete Graph

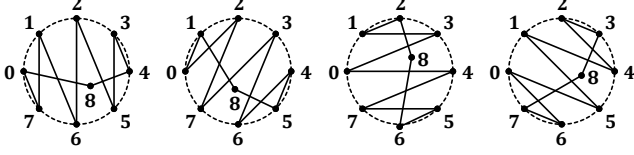


Figure 18: Hamiltonian decomposing of K_{2m+1}^* complete graph.

It has been proven that a directed complete graph K_n ($n \neq 4, 6$) can always be decomposed into $n - 1$ directed Hamiltonian cycles [11, 110]. If $n = 2m + 1$, there is a straightforward construction to decompose the graph into m undirected (bidirectional) Hamiltonian cycles. As shown in Figure 18, first, m Hamiltonian paths are constructed among $2m$ vertices by

$$(i, i - 1, i + 1, i - 2, i + 2, \dots, i + m - 1, i - m) \pmod{2m},$$

where $i = 0, \dots, m - 1$. Then, the two endpoints of each path are connected to the vertex $2m + 1$, forming a cycle. We can see that each cycle is a Hamiltonian cycle, and there is no overlap between cycles under this construction.

If $n = 2m$, the graph can be decomposed into $2m - 1$ directed Hamiltonian cycles. The construction is present in [11], which is relatively complicated and will not be illustrated here.

A.2 All-to-All-based All-Reduce

For HyperX configuration, we can perform direct reduce-scatter and all-gather algorithms on RailX based on the all-to-all interconnection. That is to say, each node sends/receives data to every other node simultaneously. The communication time of the 2D-HyperX All-Reduce algorithm is estimated as

$$T_{AR}(p, V, B) = \alpha + \frac{p-1}{p} \frac{V}{2B}, \quad (12)$$

$$\begin{aligned} T_{2D\text{-HyperX}} &= 2 \times \frac{m^2 - 1}{m^2} \frac{V}{2knB} (\text{All-Reduce on local 2D-mesh}) \\ &\quad + 2 \left[T_{AR}(p, \frac{V}{2m^2}, \frac{nB}{m}) + T_{AR}(mp, \frac{V}{2m^2p}, \frac{nB}{m}) \right] \\ &= \frac{m^2 - 1}{m^2} \frac{V}{knB} + 4\alpha + \frac{p^2 - 1}{p^2} \frac{V/m^2}{2nB/m} \\ &\approx 4\alpha + \left(\frac{2}{k} + \frac{1}{m} \right) \frac{V}{2nB}, \end{aligned} \quad (13)$$

which does not increase with the scale p .

A.3 High-Dimensional Heterogeneous Topology and Workload Mapping

A detailed example of mapping 5D parallelism on RailX is shown in Figure A.3. Tensor parallelism is mapped on the high-bandwidth 2D-mesh. Rails for expert parallelism are configured into all-to-all topology, and other rails are configured into 3D-Torus.

The communication pattern, volume, frequency, and communication time of each parallelism are shown in Table 4, where L is the layer number, B is the micro batch size, N_B is the number of micro batches per DP (global batch size $= B \times N_B \times D$), S is the sequence length, H is the hidden dimension, V is the vocabulary size, h_A and h_{KV} is the attention and key/value head number (grouped-query attention [10]), I is the intermediate dimension of FFN layers (SwiGLU activation function [103]), and K is the Top- K gating used for the MOE structure [104]. The communication time is estimated as the sum of the latency and bandwidth part, where α is the latency, T_{2D} and T_{3D} are the communication time of 2D and 3D All-Reduce.

A.4 HW/SW Configuration and Traces

To validate the analytical model, we run training workloads on real hardware and collect the trace by using NVIDIA Nsight Systems. Up to 64 NVIDIA GH200 chips [87] with 96 GB HBM3 and 120 GB LPDDR5 are used. Each scale-up node consists of four GH200 chips, all-to-all interconnected with 1.2Tb/s NVLink4.0 (six 200Gb/s links). All nodes are interconnected in a Slingshot-11 [25, 26] network with 200Gb/s NIC per each GH200 chip. Megatron-LM 0.9 (main-branch commit-7efaa73), Pytorch 3.12, NCCL 2.23.4, and CUDA 12.6 are used.

Listing 1: Parallelism and MOE configurations

```
# Parallelism Configuration
data_parallel_size: 4
tensor_model_parallel_size: 4
pipeline_model_parallel_size: 2
context_parallel_size: 2
expert_model_parallel_size: 2

# MoE Configuration
num_experts: 8
moe_router_load_balancing_type: aux_loss
moe_aux_loss_coeff: 0.01
moe_router_topk: 2
moe_token_dispatcher_type: alltoall
moe_grouped_gemm: True
```

An example trace of Llama3-70B training workload is shown in Figure 21, and the related configurations are listed

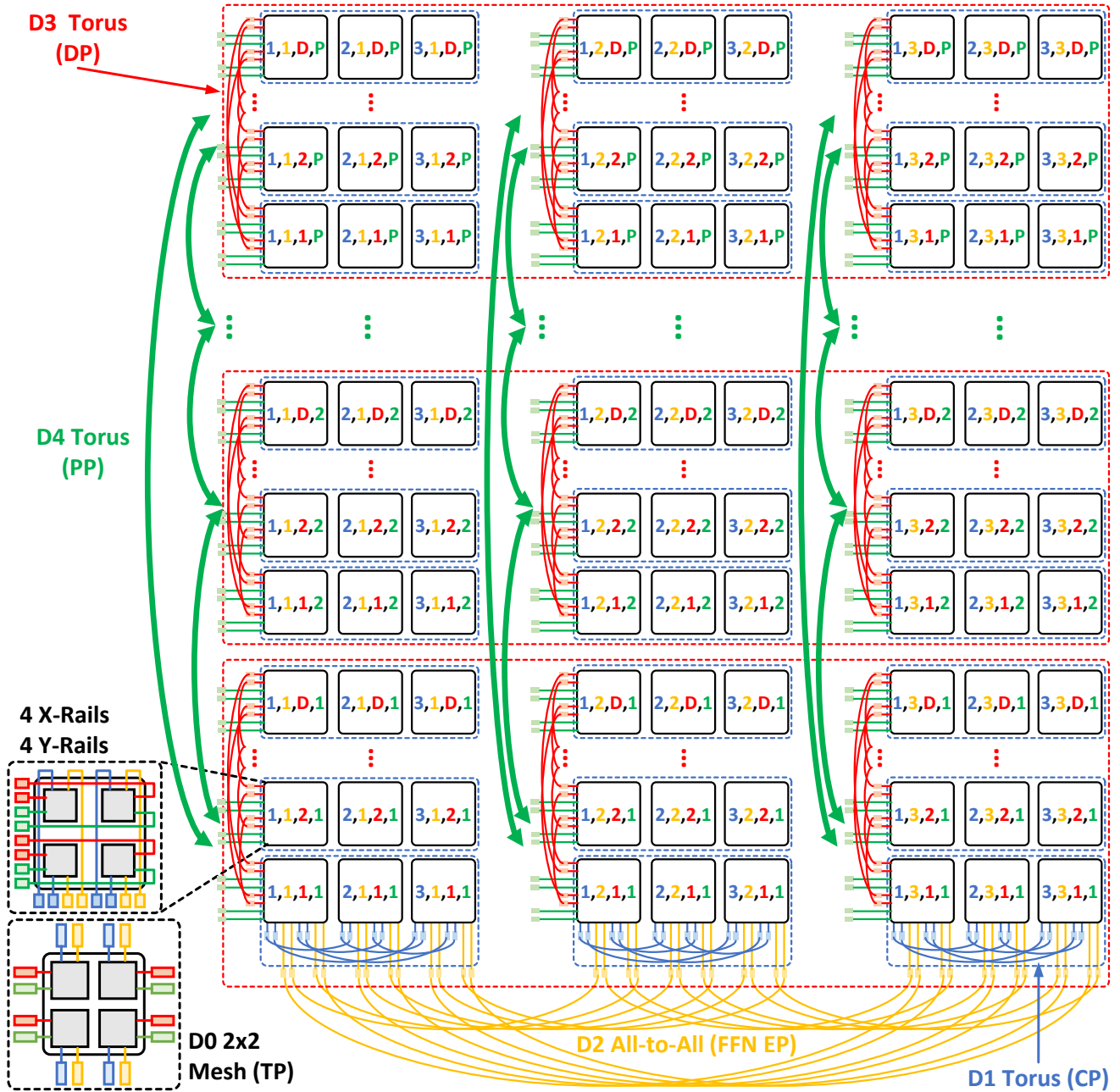


Figure 19: High-dimensional heterogeneous topology ($4 \times 3 \times 3 \times D \times P$) and the mapping of the training workload ($TP \times CP \times EP \times DP \times PP$).

in Listing 1. From the trace, we can count the actual communication and computation time of each parallelism.

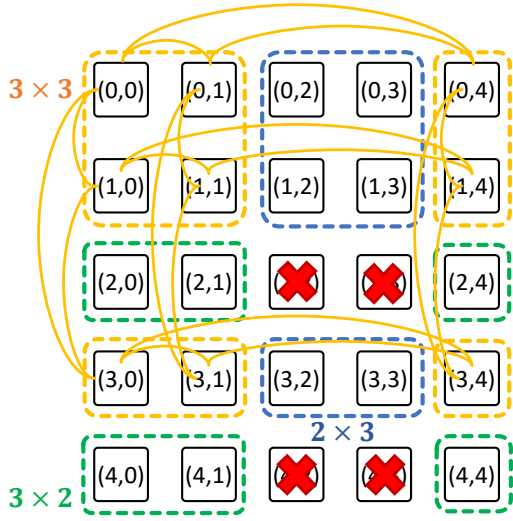
It can be measured that all-to-all communication starts 6ms after the context parallelism communication. Therefore, it is possible to configure the circuit switches in the gap between the context parallelism communication and the expert parallelism communication. Specifically, all ports of

one physical dimension are configured to connect within the CP group during the CP communication and then switch to connect within the EP group before EP communication starts. As a result, both CP and EP communications can fully utilize the bandwidth of one entire physical dimension.

Table 4: Communication scope, volume, and frequency of high-dimensional parallelism on RailX

Parallelism	Traffic Pattern	Process Group	Volume (V)	Frequency (F)	Communication Time
Tensor / SEQ (T)	Reduce-Scatter & All-Gather	$G_{T,i} = \{i, i+1, \dots, i+T_a-1\}$ (Attention Blocks)	<i>B</i> SH	$4N_B L/P$	$V/2kn \times F$
		$G_{T,i} = \{i, i+1, \dots, i+T_e-1\}$ (FFN/Expert Blocks)	<i>B</i> SHK	$4N_B L/P$	$V/2kn \times F$
Context (C)	Point-to-Point	$G_{C,i} = \{i, i+T, \dots, i+(C-1)T\}$	$BSH \times (2h_{KV}/h_A)/T$	$2N_B L/P$	$(C\alpha + V/\frac{2n_c}{m}) \times F$
Expert (E)	All-to-All	$G_{E,i} = \{i, i+TC, \dots, i+(E-1)TC\}$	<i>B</i> SHK/TC	$4N_B L/P$	$(\alpha + V/\frac{2n_e}{m}) \times F$
Data ($D = ED_e$)	All-Reduce	$G_{D_{VOC},i} = \{i, i+TC, \dots, i+(D-1)TC\}$	$2HV/TC$	1	$T_{2D}(n_e, n_d) \times F$
	All-Reduce	$G_{D_{QKV},i} = \{i, i+T, \dots, i+(CD-1)T\}$	$(2+2h_{KV}/h_A)H^2/T$	L/P	$T_{3D}(n_e, n_e, n_d) \times F$
	All-Reduce	$G_{D_{FFN},i} = \{G_{C,i}, G_{C,i+TCE}, \dots, G_{C,i+(D_e-1)TCE}\}$	$3HI/T$	L/P	$T_{2D}(n_e, n_d) \times F$
Pipeline (P)	Point-to-Point	$G_{P,i} = \{i \Leftrightarrow i+TCD \Leftrightarrow \dots \Leftrightarrow i+(P-1)TCD\}$	<i>B</i> SH/TC	$2N_B$	$V/\frac{n_p}{m} \times F$

A.5 Allocating Jobs on RailX with Faulted Nodes


Figure 20: Allocation of jobs with failure nodes.

In the MLaaS scenario, we can use multiple small workloads to fully utilize all functional nodes in the faulted *RailX*. As shown in Figure 20, four faulted nodes are marked with red crosses. If using *RailX* for a single job, two entire rows or columns of nodes must be disconnected to work around the faulted nodes. However, when multiple small jobs are allocated, three sub-networks fully utilize all the functional nodes.

The general allocation has been proven to be a NP-hard problem [48]. However, since the faulted nodes are sparse, which means they rarely appear in the same row or column, we can use a fast algorithm to find the maximum available single-allocation size. As shown in Algorithm 2, we first find all non-isolated faulted nodes (appearing in the same row or column with other faulted nodes) and isolated faulted nodes. Then, we iterate over all cases for non-isolated faulted nodes to disable rows or columns by complexity $O(2^{|C|})$; for each

Algorithm 2 MAXIMUM AVAILABILITY IN FAULTED GRID

Input: System size: $n \times n$;

Faulted nodes: $F = \{(r_i, c_i)\}$.

Output: Maximum available single-allocation size.

- 1: $I \leftarrow$ Isolated faulted nodes
 - 2: $C = F - I \leftarrow$ Non-isolated faulted nodes
 - 3: **if** C is \emptyset **then** // all nodes are isolated
 - 4: // evenly disable rows and columns
 - 5: **return** $(n - \text{ceil}(|F|/2)) \times (n - \text{floor}(|F|/2))$
 - 6: **end if**
 - 7: $S_{\max} \leftarrow 0$
 - 8: // Iterate over all cases for C (0/1: disable row/column)
 - 9: **for each** $\in \{0, 1\}^C$ **do**
 - 10: $r_i \leftarrow$ disabled rows
 - 11: $c_i \leftarrow$ disabled columns
 - 12: Adjust $|I| = r' + c'$ ($r', c' \in N$)
 - 13: $S \leftarrow \max_{r', c'} [(n - r_i - r') \times (n - c_i - c')]$
 - 14: $S_{\max} \leftarrow \max(S_{\max}, S)$
 - 15: **end for**
 - 16: **return** S_{\max}
-

case, we maximize the available size by making width and height as close as possible. Finally, we return the maximum available size. Since the failure rate is low, faulted nodes are sparse, so $|C|$ is supposed to be small, and the algorithm is efficient.

A.6 Chiplet Network Simulator

A sophisticated 2D-mesh is adopted within each node, whose performance is tightly linked to microarchitecture and routing algorithms. Fine-grained network simulation can be very slow [56, 65] (days to simulate more than 1K chips). *Chiplet Network Simulator (CNSim)* is a recent cycle-accurate simulator that supports multi-threading simulation [37].

What we model by using CNSim includes router pipelines, virtual cut-through packet switching, fine-grained VC-based deterministic/adaptive routing algorithms, and non-uniform link bandwidth/latency. To speed up the simulation, we enable multi-threading, omit network protocols (e.g., TCP/IP),

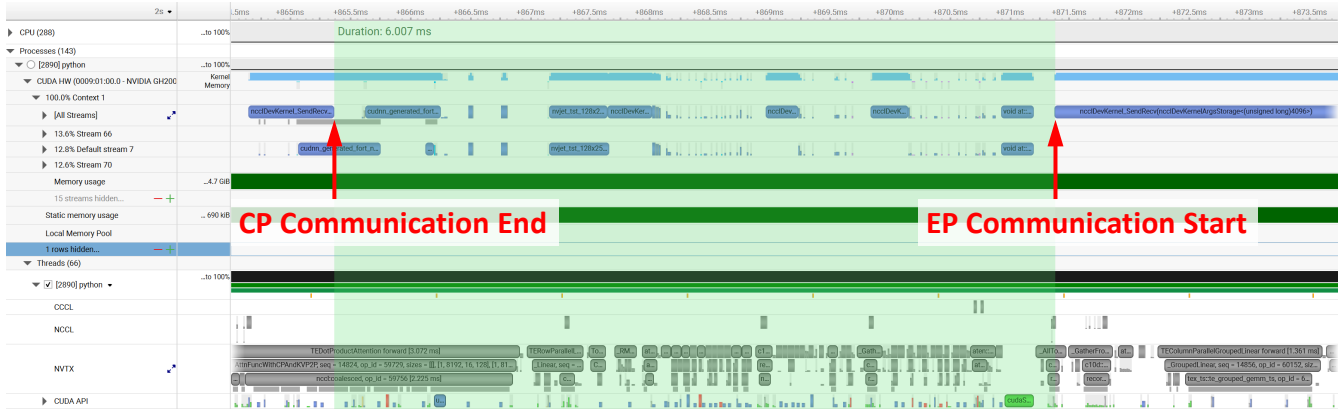


Figure 21: Trace example. CP and EP are separated by 6 ms.

and use simplified link delay. The default parameters used in simulations are shown in TABLE 5.

Table 5: Default Parameters

Parameter	Value
Packet Length	4 flits
Input Buffer Size	16 flits
Base Link Bandwidth	1 flit/cycle
Short-Reach Link Delay	1 cycle
Long-Reach Link Delay	10 cycles
Simulation Time	10000 cycles after 5000 cycles warming up

A.7 Cost

Detailed cost results are shown in Table 6, which includes the number of switches, passive copper cables (PCCs), and active optical transceivers (AOTs). Since all topologies can achieve near-bandwidth-optimal All-Reduce with proper algorithms, the cost per injection bandwidth approximates the cost per All-Reduce bandwidth. With 64-port packet switches, 2-tier non-blocking Fat-Tree can only connect 2048 chips, the cost of which is regarded as baseline. By over-subscribing the switches, 3:1 Taper Fat-Tree can connect 3072 chips at a lower cost, but the global bisection bandwidth is only one-third of the non-blocking Fat-Tree, so the cost per global bandwidth is higher. With 128-port circuit switches, the cost of which is assumed to be the same as the 64-port packet switch, RailX4Mesh can connect 65536 chips with 12.5% of the bisection bandwidth, and RailX7Mesh can connect 200704

chips with 7.1% of the bisection bandwidth. As a result, RailX achieves much higher scalability with a much lower cost per injection bandwidth while maintaining a similar cost per global bandwidth.

To achieve the same scale as the 128-port-OCS-based RailX7Mesh (~ 200K chips), four tiers of switches are required, costing more than two times the 2-tier Fat-Tree. By using the 49:7:1 Taper Fat-Tree, we can reduce the number of tiers to three, but the cost per global bisection bandwidth will be significantly higher.

A.8 Related Work

BML [115] is a network architecture based on the BCube topology [47]. It achieves higher All-Reduce bandwidth with fewer switches than the traditional Fat-Tree-based parameter server. However, only data parallelism is considered in BML, which is insufficient for the modern hyper-scale LLM training workload.

TopoOpt [117] and SiP-ML [62] are two recent reconfigurable network architectures for ML training. They both use commercially available optical circuit switches and online/off-line methods to optimize the network topology for specific workloads. However, their scalability is limited by the radix of optical switches, and they are not optimized for all-to-all communication, which is essential for MOE models.

Rail-Only removes all cross-rail switches in traditional rail-optimized Fat-Tree and uses a scale-up network for cross-rail communication. From the topology perspective, Rail-only is a 2D Fat-Tree (scale-up and scale-out). In § 6.2, we let the two Fat-Tree networks have the same bandwidth because this leads to the best global All-to-All throughput.

Table 6: Cost comparison with 64-port packet switches and 128-port circuit switches. Each chip has 36 ports.

Topology	Scale [#]	Switch [#]	PCC [#K]	AOT [#K]	Cost [M\$]	Cost [/Inject]	Glob. BW [% Inject]	Cost [/GBW]
2-Tier Nonbl. FT	2048	3456	0	294.9	415.9	1×	100	1×
1:3 Tap. 2-Tier FT	3072	2880	0	294.9	395.7	0.65×	33.3	1.90×
Hx4Mesh (1-Tier FT)	16384	2304	0	294.9	375.6	0.11×	12.5	0.90×
Hx7Mesh (1-Tier FT)	50176	4032	0	516.1	657.2	0.06×	7.1	0.91×
3D-Torus w/ OCS	4096	288	30.7	36.9	185.7	0.22×	4.2	5.52×
3D Torus w/o OCS	4096	0	30.7	36.9	45.0	0.05×	4.2	1.46×
Rail-Only (2D FT)	4096	2304	0	294.9	375.6	0.45×	50	0.90×
RailX4Mesh	65536	4608	0	589.8	751.1	0.06×	12.5	0.45×
RailX7Mesh	200704	8064	0	1032.2	1314.4	0.03×	7.1	0.45×
4-Tier Nonbl. FT	196608	774144	0	56623	83718	2.10×	100	2.10×
1:7:49 Tap. 3-Tier FT	200704	149760	0	16810	22052	0.54×	2.0	26.5×
Hx7Mesh (2-Tier FT)	200704	48384	0	4128	5822	0.14×	7.1	2.01×